PTUPB, a soluble epoxide hydrolase/cyclooxygenase-2 dual inhibitor, reduces endothelial-to-mesenchymal transition and improves doxorubicin-induced vascular and cardiac toxicity

HEVNA DHULKIFLE[1], LUBNA THERACHIYIL[1,2], MARAM H. HASAN[3], SHAHD M. YOUNIS[2], NIZAR A. AL-SHAR'I[1], HUSEYIN C. YALCIN[3,4] and ZAID H. MAAYAH[1]

[1]Department of Pharmaceutical Sciences, College of Pharmacy, QU Health, Qatar University, Doha 2713, Qatar; [2]Translational Research Institute, Hamad Medical Corporation, Doha 3050, Qatar; [3]Biomedical Research Center, QU Health, Qatar University, Doha 2713, Qatar; [4]Department of Biomedical Sciences, College of Health Sciences, QU Health, Qatar University, Doha 2713, Qatar

Received March 18, 2025; Accepted September 11, 2025

DOI: 10.3892/mmr.2026.13810

Abstract. Doxorubicin (DOX) is an effective anthracycline agent used to combat a number of neoplastic diseases. However, DOX causes cardiovascular toxicity in juvenile and young adult survivors of cancer that can lead to future cardiomyopathy. Thus, it is important to address the cardiovascular toxicity caused by DOX to improve the long-term health of patients with cancer. Soluble epoxide hydrolase (sEH) and cyclooxygenase-2 (COX-2) are implicated in cardiovascular diseases by impairing vascular health and promoting the transition of endothelial cells to mesenchymal cells. Given the role of sEH and COX-2 in endothelial-to-mesenchymal transition (EndMT)-derived cardiovascular toxicity, the present study aimed to investigate the effect of a dual sEH/COX-2 inhibitor, 4-[5-phenyl-3-[3-[[[[4-(trifluoromethyl)phenyl] amino]carbonyl]amino]propyl]-1H-pyrazol-1-yl]-benzenesulfonamide (PTUPB), on DOX-induced EndMT-derived vascular and cardiac toxicity. The mitigating effect of PTUPB on DOX-induced cardiovascular toxicity was explored in zebrafish. The cardiovascular parameters were measured using the Viewpoint MicroZebralab software. Additionally, the effect of PTUPB on DOX-induced EndMT was assessed in human endothelial cells. The data from the present study indicated that the inhibition of sEH and COX-2 using PTUPB reduced DOX-induced EndMT and vascular toxicity. The data also demonstrated that PTUPB improved cardiac function and morphology in zebrafish incubated with DOX. The results of the present study showed that PTUPB downregulated inflammation and oxidative stress markers, which contributed to the improvement in DOX-induced cardiovascular toxicity. In conclusion, the findings of the present study indicated that the suppression of sEH/COX-2 using PTUPB reduced DOX-induced EndMT and the resulting vascular and cardiac toxicity.

Correspondence to: Dr Zaid H. Maayah, Department of Pharmaceutical Sciences, College of Pharmacy, QU Health, Qatar University, Al Dafna, 233 Al Jamia Street, Doha 2713, Qatar
E-mail: almaayah@qu.edu.qa

Key words: doxorubicin, cardiovascular, endothelial cells, dihydroxyeicosatrienoic acid

Introduction

Anthracycline antibiotics such as doxorubicin (DOX) are one of the most potent types of chemotherapy used to treat different types of tumors, including breast cancer, lymphoma, and leukemia (1,2). However, the number of individuals who are at risk of anthracycline-induced cardiovascular damage is growing, due to the increasing use of anthracyclines and an advancement in detection methods (1). The increased risk of cardiovascular complications following anthracycline chemotherapy, compared with other chemotherapy drugs or no treatment, is a leading cause of morbidity and mortality in the cancer population (1,3,4). Considering the potential impacts of cardiovascular toxicity induced by anthracycline treatments in patients with cancer, protecting the cardiovascular system from this detrimental effect would increase the favorability of the risk-benefit ratio of treatment with anthracycline and result in improved survival outcomes. Thus, implementing measures to decrease the incidence of anthracycline-induced cardiovascular toxicity is important.

One of the strategies to reduce the incidence of anthracycline-induced cardiovascular toxicity, and thus, the cost and burden on the healthcare system, is to improve understanding of the molecular pathways that serve an important role in the development of anthracycline-induced cardiovascular toxicity. Previous studies have focused on the vascular system and vascular endothelium as important targets of the cardiovascular toxicity induced by DOX (5,6). Since DOX is administered intravenously, the vascular system and vascular endothelium are the first contact points for DOX within the patient (7). Thus, it is reasonable to assume that endothelial and vascular toxicity may occur

earlier in the treatment with DOX and be an antecedent for DOX-induced cardiovascular toxicity (5,6,8). Consistent with this, DOX-treated juvenile and young adult survivors of cancer exhibit impaired endothelial and vascular function, and an increased incidence of cardiovascular diseases later in life (5,6). However, the pathogenic mechanisms responsible for endothelial and vascular toxicity induced by DOX remain ambiguous.

Vascular endothelial cells secrete small molecules that contribute to the homeostasis of the cardiovascular system. Among these small molecules, epoxyeicosatrienoic acids (EETs), products of cytochrome p450 epoxygenases (CYP epoxygenases), serve an important role in maintaining endothelial and vascular function (9,10). Notably, EETs are endothelium-derived hyperpolarizing factors that have antiplatelet (11) and antiapoptotic properties (12), reduce the frequency and the likelihood of endothelial-to-mesenchymal transition (EndMT), reduce endothelial and vascular dysfunction, and inhibit vascular smooth muscle cell proliferation (13-15). EETs have also been reported to possess anti-inflammatory (16,17), antihypertensive, antihypertrophic and potential anti-fibrotic effects (18,19). Conversely, the downregulation of CYP epoxygenases and the resulting reduction in EETs exacerbate endothelial inflammation, aggravate EndMT, and worsen vascular and cardiac dysfunction (20). Thus, targeting the EET signaling axis may help to reduce DOX-induced EndMT and vascular toxicity, and thereby improve cardiovascular function.

While several CYP epoxygenases, including the CYP2B, CYP2C and CYP2J subfamilies, can produce four regioisomeric EETs (5,6-, 8,9-, 11,12- and 14,15-EET) from the EET precursor arachidonic acid (9,10), EETs are rapidly metabolized by soluble epoxide hydrolase (sEH) into the corresponding less active dihydroxyeicosatrienoic acid (DHET) molecules and by cyclooxygenase-2 (COX-2) into carcinogenic products, epoxyhydroxyeicosatrienoic acids (EHETs) (21,22). The dual inhibition of sEH and COX-2 enzymes using 4-[5-phenyl-3-[3-[[[[4-(trifluoromethyl)phenyl]amino]carbonyl]amino] propyl]-1H-pyrazol-1-yl]-benzenesulfonamide (PTUPB) causes EETs to accumulate, and markedly reduces EndMT, improves blood pressure, and abrogates endothelial, liver, renal and lung injury and inflammation (22,23) However, it remains ambiguous whether or not the dual inhibition of sEH and COX-2 enzymes using PTUPB will reduce DOX-induced EndMT, and vascular and cardiac toxicity. Therefore, the present study aimed to test the hypothesis that dual inhibition of the EET-metabolizing enzymes, sEH and COX-2, using PTUPB would protect against endothelial and cardiovascular toxicity induced by DOX.

Materials and methods

Cell culture. MDA-MB-231 cells (cat. no. HTB-26; American Type Culture Collection) and EA.hy926 human endothelial cells (cat. no. CRL-2922; American Type Culture Collection) were cultured in 75-cm^2 tissue-culture flasks that contained Dulbecco's Modified Eagle Medium F-12 Nutrient Mixture supplemented with 10% w/v fetal bovine serum and 1% w/v Antibiotic-Antimycotic (all Gibco; Thermo Fisher Scientific, Inc.) in a humid environment at 37˚C with 5% CO_2.

Cell viability. EA.hy926 cells and MDA-MB-231 were incubated with 1, 2.5, and 5 μM of PTUPB (Item No. 10897, Cayman Chemical) for 24 h or 2 μM DOX (Item No. 0069-0277-02, Pfizer Inc) alone or in combination with 1, 2.5, or 5 μM of PTUPB for 24 h. In all experiments, the control cells were incubated with a comparable volume of vehicle [Dimethyl sulfoxide (DMSO) 0.1% v/v (cat. No. PI85190; Thermo Fisher Scientific]. All treatments were performed in a humid environment at 37˚C with 5% CO_2. The MTT assay was then performed as described previously (24). The percentage of viable cells was calculated relative to healthy control cells.

Cell morphology. To assess EndMT, EA.hy926 human endothelial cells were treated with 2 μM DOX alone or in combination with 1 μM PTUPB for 24 h. Control cells were incubated with a comparable volume of vehicle DMSO 0.1% v/v (cat. no. PI85190; Thermo Fisher Scientific). All treatments were performed in a humid environment at 37˚C. Morphological images of EA.hy926 cells were captured at a magnification of x10 (scale bar, 100 μm) using a 'SteREO Discovery V8 light microscope' (Carl Zeiss AG). As previously described (20,25), the proportion of mesenchymal cells (long, spindle-like cells) to endothelial cells (cobblestone monolayer-like cells) was measured using AxioVision Imaging software 4.8.2 (Carl Zeiss AG).

Measurement of DHET levels. Since EET is rapidly metabolized by sEH into DHET, the effect of PTUPB on the sEH enzyme was measured at the activity level by examining the levels of DHET formation. Cells were treated with 2 μM DOX and/or 1 μM PTUPB for 24 h and then incubated with 0.5 μM EET for 1 h in a dark environment. In all experiments, the control cells were incubated with a comparable volume of vehicle DMSO 0.1% v/v (cat. no. PI85190; Thermo Fisher Scientific, Inc.). All treatments were performed in a humid environment at 37˚C with 5% CO_2. DHET levels were measured using the 14,15 EET/DHET ELISA Kit (Cat No. ab175812; Abcam) according to the manufacturer's protocol.

Measurement of cardiovascular function and structure in zebrafish. The zebrafish experiments were conducted in accordance with international guidelines and the policies required by Qatar University (Doha, Qatar) and the Department of Research in the Ministry of Public Health for the use of zebrafish in experimental studies, with the approval of the Institutional Animal Care and Use Committee (approval no. QU-IACUC 006/2023-AMM1), (Qatar University, Doha, Qatar).

As previously described (26), 360 wild-type zebrafish embryos (AB strain) were grown in a 10-mm petri dish with E3 medium at 28.5˚C under typical aquaculture conditions and a 14 h light/10 h dark cycle. The zebrafish embryos were generated and supplied by the Zebrafish Facility at Qatar University under approval number (QU-IACUC 006/2023-AMM1). The method of generating zebrafish embryos was as described previously (27). The E3 medium was freshly prepared as described previously (28).

The zebrafish embryos were randomly sorted into four groups (n=10/group) at 24 h post-fertilization (24 hpf), and incubated for 72 h with vehicle, 100 μM DOX (Item No.

0069-0277-02, Pfizer Inc.), 1 μM PTUPB (Item No. 10897, Cayman), or a combination of 100 μM DOX and 1 μM PTUPB . In another experiment, a distinct set of zebrafish embryos was randomly divided into four groups (n=10/group) at 24 hpf, and incubated for 72 h with either vehicle, 100 μM DOX, 1 μM 4-[[trans-4-[[(tricyclo[3.3.1.13,7]dec-1-ylamino) carbonyl]amino]cyclohexyl]oxy]-benzoic acid (t-AUCB) (Item no. 16568, Cayman) or a combination of 100 μM DOX and 1 μM t-AUCB. Lastly, an additional set of zebrafish embryos was divided into four groups (n=10/group) at 24 hpf, and incubated for 72 h with either vehicle, 100 μM DOX, a combination of 100 μM DOX and 1 μM PTUPB, or a combination of 100 μM DOX, 1 μM PTUPB, and 50 μM N-methylsulfonyl-6-(2-propargyloxyphenyl)-hexanamide (MSPPOH; cat. No. 75770, Cayman), an EET formation inhibitor. All experiments were performed at 28.5˚C under typical aquaculture conditions and a 14 h light/10 h dark cycle. In all experiments, the control cells were incubated with an equal volume of vehicle DMSO 0.1% v/v (cat. no. PI85190; Thermo Fisher Scientific).

In all experimental models, over a period of 3 days, the survival and morphological changes of the zebrafish were noted every 24 h. Hatching, survival, and any morphological or developmental alterations were monitored and documented using a 'SteREO Discovery V8 light microscope (Carl Zeiss AG) with a Hamamatsu Orca Flash camera (Hamamatsu Photonics UK Limited) and HCImage software 2.0.4 (Hamamatsu Photonics UK Limited)'. When non-viable embryos were found, they were immediately removed. As previously described (20,29), the morphology, survival rate, and cardiovascular health of treated fish were assessed at 72 hpf. We utilized version 3.6 of the MicroZebralab software (Viewpoints) to measure the diameter of the dorsal aorta (DA) and the posterior cardinal vein (PCV), as well as to assess blood flow velocity as described previously (27,29). The formulas shown in Table SI were used to determine the cardiovascular functional parameters, as previously described (Table SI) (20,29). Given that the zebrafish larvae used were <5 dpf, the fish were euthanized at 72 h post fertilization by hypothermic shock as per American Veterinary Medical Association guidelines (30,31). Briefly, larvae were submerged in ice-cold water (0-4˚C; 5:1 ratio of ice to water) for 20 min. Secondary euthanasia was performed by adding 1 part of 6.15% sodium hypochlorite (bleach) to 5 parts of E3 culture medium containing the larvae and allowing them to remain submerged for 10 min (31).

The DOX concentration of 100 μM used in the zebrafish model in the present study was selected based on the previous literature showing that DOX consistently induces cardiotoxicity in zebrafish at this concentration (26,32,33). Additionally, given that DOX was administered at 24 hpf, a high concentration of DOX was necessary for uptake by the chorion and its accumulation inside the fish (34). The concentration of PTUPB was chosen based on the maximum non-toxic concentration of PTUPB in combination with DOX in the endothelial cells, as well as another previous study that showed that treatment with ~30 mg/kg PTUPB results in a 1 μM blood plasma level within these mice and was not associated with toxicity (35). Lastly, the concentration of the EET formation inhibitor MSPPOH was selected based on our previous experiment using zebrafish (20).

Reverse transcription-quantitative PCR (RT-qPCR). Total RNA was isolated from MDA-MB-231 cells, EA.hy926 human endothelial cells and entire zebrafish larvae using TRIzol® reagent (Invitrogen; Thermo Fisher Scientific, Inc.) as described previously (20,24). The concentration and purity of the total RNA were measured using a nanospectrophotometer. The High-capacity cDNA RT kit (Applied Biosystems; Thermo Fisher Scientific, Inc.) was used to synthesize the corresponding cDNA from the RNA according to the manufacturer's instructions. As described previously (36), the Applied Biosystems QuantStudio™ 5 Real-Time PCR System, Fluorophore: FAM™ (Applied Biosystems; Thermo Fisher Scientific, Inc.) was used to quantify mRNA expression. Thermocycling conditions were as follows: 'Initial denaturation step at 95˚C for 15 sec, followed by 40 amplification cycles of denaturation at 95˚C for 15 sec, followed by a combined annealing and extension phase at 60˚C for 30 sec'. Luna® Universal qPCR Master Mix reagent (New England Biolabs) was used in our experiment. Primers for RT-qPCR were obtained from Invitrogen (Thermo Fisher Scientific, Inc.). Table SII lists the primer sequences utilized in the current study. As previously described (36), RT-qPCR data were analyzed using the $2^{-\Delta\Delta Cq}$ method (37). The fold change in mRNA expression was normalized using reference primers, specifically β-actin for human cells and ribosomal protein L13a for zebrafish.

Whole proteome extraction. The AB strain zebrafish embryos were treated with vehicle (DMSO), 100 μM DOX alone or 100 μM DOX combined with 1 μM PTUPB for 72 h. All experiments were performed at 28.5˚C. Protein was then extracted from the whole zebrafish larvae. Briefly, the embryos were transferred into a microcentrifuge tube with three tubes designated for each treatment group. Each tube contained eight embryos. RIPA buffer (Invitrogen; Thermo Fisher Scientific, Inc.) supplemented with a halt protease-phosphatase inhibitor cocktail (1X) and stored on ice was then added. The fish were homogenized, incubated for 30 min on ice, and centrifuged at 14,000 x g for 15 min at 4˚C. The extract was then transferred into a fresh Eppendorf tube. Finally, a Rapid Gold BCA assay kit (Thermo Fisher Scientific, Inc.) was used to quantify the protein as described previously (38,39).

Liquid chromatography-tandem mass spectrometry (LC-MS/MS) analysis. A previously described method was used to prepare the protein samples for the LC-MS/MS analysis (20,38). Briefly, we employed the timsTOF Pro Mass Spectrometer (Bruker) utilizing electrospray ionization (ESI) under specific conditions: a nitrogen gas temperature of 2200˚C, a nebulizer pressure of 4 bar, and a nitrogen gas flow rate of 10 l/min. Data acquisition was conducted in data-dependent mode, which dynamically selects the top ten most abundant precursor ions from the survey scan range of 400-1,800 m/z for fragmentation and MS/MS analysis. Precursors with a +1 charge state were excluded, and dynamic exclusion was applied for a duration of 25 sec.

MS and LC-MS/MS data processing and analysis. MaxQuant (maxquant.org, version 2.1.4.0) in-built search engine Andromeda (40) was utilized to analyze the MS/MS raw data using a standard workflow (41). The

UniProtKB/Swiss-Prot zebrafish database (https://www.uniprot.org/proteomes/UP000000437) was used to identify proteins (38). The 'MaxLFQ label-free quantitation method' was utilized in MaxQuant (42). Normalized label-free quantification (LFQ) spectral intensity was then used to quantify the protein levels. Following data importation from the MaxQuant analysis into the Perseus program ((https://maxquant.net/perseus/), version 2.0.11.), the LFQ intensities were transformed into $\log_2(x)$ in accordance with a previously described procedure (20,38). Values from the normal distribution 'width=0.3, downshif=1.8' were used to replace each missing LFQ intensity value. Lastly, a two-tailed unpaired Student's t-test with a permutation-based false discovery rate of 5% was used to calculate the statistical significance ($P>0.05$).

Computational study of PTUPB. All modeling steps in the present computational study were conducted using Discovery Studio® 2025 from Biovia (Dassault Systèmes S.E.). The chemical structures of PTUPB, 4-[5-(4-methylphenyl)-3-(trifluoromethyl)-1H-pyrazol-1-yl]-benzenesulfonamide (celecoxib) and trans-AUCB were sketched using ChemDraw Professional 16.0 (revvitysignals.com/products/research/chemdraw) (Fig. S1), and the structural models of human COX-1, COX-2 and sEH were obtained from the Protein Data Bank (PDB, (https://www.rcsb.org/)) using accession codes 6Y3C (resolution of 3.36 Å; apo protein), 5KIR (resolution of 2.7 Å; complexed with rofecoxib) and 5AI9 (resolution of 1.80 Å; complexed with synthetic inhibitor K78), respectively. The structural models of the zebrafish COX-2 (z-COX-2) and sEH proteins were obtained as AlphaFold (version no. 2)-generated homology models from the UniProt database (https://www.uniprot.org) using accession codes Q8JH43 and Q5PRC6, respectively (alphafold.ebi.ac.uk/).

The sequence alignment of proteins was conducted using the Align Sequences protocol available in Discovery Studio® 2025 from Biovia (Dassault Systèmes S.E.).

Docking of PTUPB into the target proteins was conducted using the CDOCKER protocol (with pharmacophore restraints for COX-2 isoforms) within Discovery Studio, following a previously reported procedure (43). Briefly, all proteins were prepared, solvated, and then sequentially minimized. The co-crystallized inhibitors, whenever a complex was available, were extracted and redocked into their respective binding sites as a docking validation step. To define the active sites of the zebrafish homology-modeled enzymes, they were superimposed on their respective human congeners, and the co-crystalized ligands were copied to the homology models and used to define their active sites prior to ligand (PTUPB and trans-AUCB) docking. The sphere defining the binding sites of the two isoforms of the two proteins was set to 10 Å to encompass all amino acids relevant to ligand binding.

Statistical analysis. GraphPad Prism (version 7.04; Dotmatics) was used for statistical analysis. The results are presented as the mean ± SEM of ≥3 independent experimental repeats. A two-tailed unpaired Student's t-test with a permutation-based false discovery rate of 5% was used to calculate the statistical significance in proteomic analysis. One-way ANOVA followed by Tukey-Kramer's post hoc multiple comparison test was used to assess the differences between groups. $P<0.05$ was considered to indicate a statistically significant difference.

Results

PTUPB reduces DOX-induced sEH and COX-2 expression in human endothelial cells. To assess whether the human endothelial cell line model used in the present study expressed sEH and COX-2, the basal expression levels of sEH and COX-2 in EA.hy926 cells were measured. The results showed that both sEH and COX-2 were constitutively expressed in the EA.hy926 cells (Fig. 1A). Following incubation of these endothelial cells with DOX, the EA.hy926 cells exhibited concentration-dependent upregulation of the mRNA expression levels of sEH (Fig. 1B) and COX-2 (Fig. 1C) in comparison with the control. Since 2 μM DOX exhibited the greatest effect on the expression levels of sEH and COX-2 in EA.hy926 cells, this concentration was used in all subsequent experiments.

To test the effect of PTUPB on DOX-induced sEH and COX-2 expression, endothelial cells were treated with 0.0, 1.0, 2.5 and 5.0 μM PTUPB either alone or in combination with 2 μM DOX. Based on the cell viability assay, a PTUPB concentration of 1 μM was chosen for subsequent experiments, as this concentration exhibited a non-significant difference in EA.hy926 cell viability compared with the control group (Fig. 1D) or in the presence of 2 μM DOX (Fig. 1E). Using this concentration, PTUPB was shown to significantly downregulate DOX-induced sEH (Fig. 1F) and COX-2 (Fig. 1G) expression in EA.hy926 cells treated with DOX. In addition, PTUBP significantly decreased the DOX-induced formation of DHETs (Fig. 1H), suggesting that PTUBP inhibited the enzyme activity of sEH in EA.hy926 cells. Overall, the present data indicated that PTUPB decreased the upregulation of sEH and COX-2 expression induced by DOX in human endothelial cells.

Inhibition of sEH and COX-2 using PTUPB attenuates DOX-induced EndMT. Given that DOX induces EndMT in endothelial cells (20,25), the present data showed that DOX upregulated sEH and COX-2 expression in EA.hy926 cells (Fig. 1), and that sEH and COX-2 are known to detrimentally affect the function and structure of vascular endothelial cells by promoting the transition of endothelial cells to mesenchymal cells (44,45), we hypothesized that DOX may induce EndMT and endothelial toxicity via the upregulation of sEH and COX-2. If this was the case, it would be expected that inhibition of sEH and COX-2 would reduce DOX-induced EndMT and endothelial toxicity. To test this hypothesis, the mRNA expression levels of EndMT markers were measured in EA.hy926 cells incubated with DOX with or without PTUPB. Notably, DOX was shown to significantly increase the expression levels of a number of EndMT markers, including smooth muscle actin α2 (ASMA; Fig. 2A), smooth muscle protein 22α (SMA22; Fig. 2B), vimentin (VIM; Fig. 2C), cadherin-2 (CDH2; Fig. 2D), TGF-β (Fig. 2E), snail family transcriptional repressor 1 (SNAI1; Fig. 2F) and snail family transcriptional repressor 2 (SNAI2; Fig. 2G), and significantly decreased the expression levels of the endothelial marker CD31 (Fig. 2H), compared with those in the control group. Notably, the data showed that PTUPB, a dual inhibitor of sEH and COX-2,

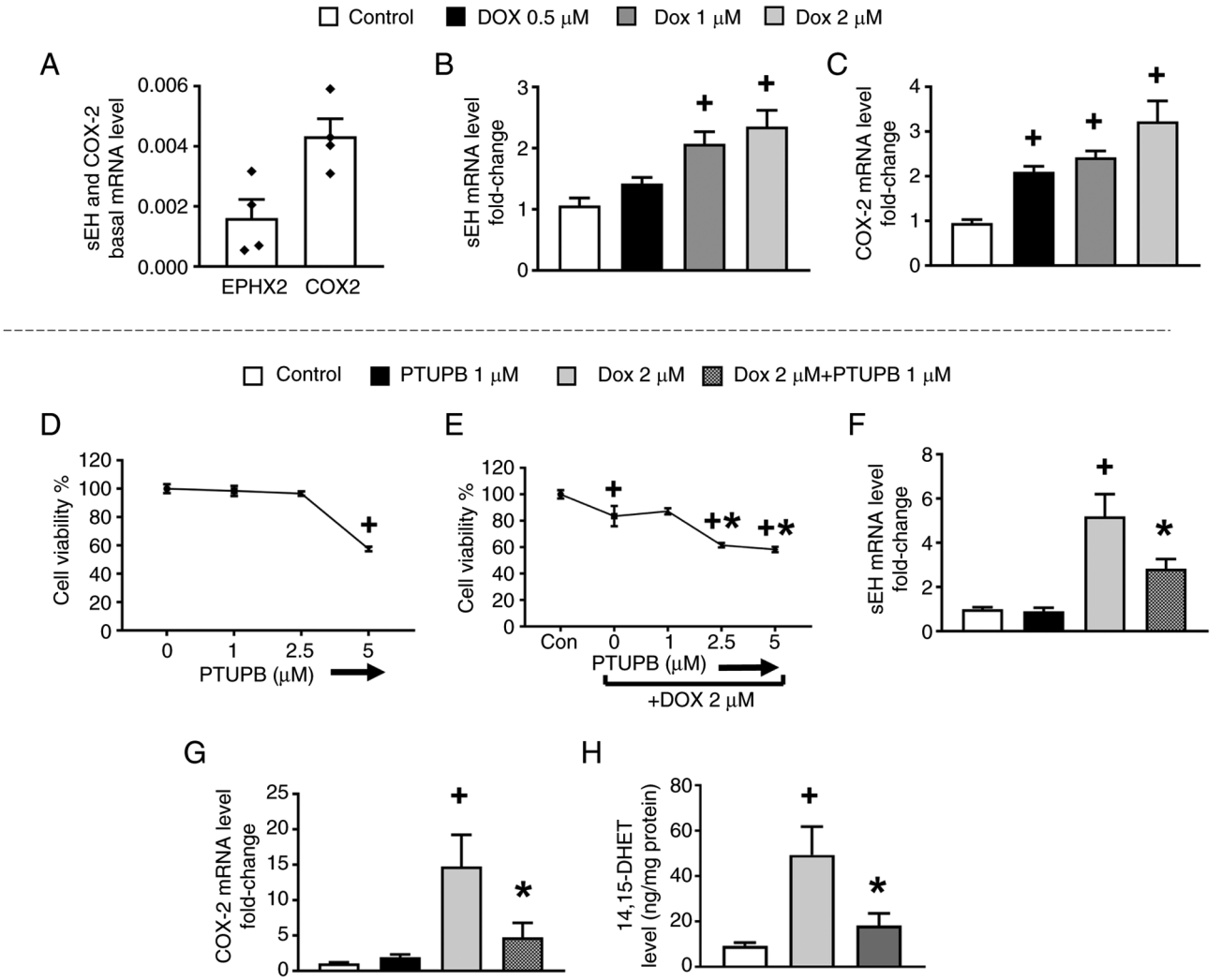

Figure 1. PTUPB decreases DOX-induced sEH and COX-2 expression in human endothelial cells. (A) Basal gene expression levels of sEH and COX-2 in endothelial cells. EA.hy926 cells were treated with 0.5 μM, 1 μM and 2 μM DOX for 24H. Gene expression levels of (B) sEH and (C) COX-2 in DOX-treated cells. Viability of EA.hy926 cells treated with either (D) PTUPB alone or (E) in combination with DOX. EA.hy926 cells were treated with 2 μM DOX with or without 1 μM PTUPB for 24 h. Gene expression levels of (F) sEH and (G) COX-2. (H) Activity level of sEH. One-way ANOVA followed by Tukey's multiple comparison tests was performed. $^{+}$P<0.05 vs. control, *P<0.05 vs. DOX). sEH, soluble epoxide hydrolase; COX-2, cyclooxygenase-2; DOX, doxorubicin; PTUPB, 4-[5-phenyl-3-[3-[[[[4-(trifluoromethyl)phenyl]amino]carbonyl]amino]propyl]-1H-pyrazol-1-yl]-benzenesulfonamide; DHET, dihydroxyeicosatrienoic acid; Con, control.

significantly downregulated the expression levels of EndMT markers, including ASMA (Fig. 2A), SMA22 (Fig. 2B), VIM (Fig. 2C), CDH2 (Fig. 2D), SNAI1 (Fig. 2F), and SNAI2 (Fig. 2G), and significantly upregulated the expression levels of the endothelial marker CD31 (Fig. 2H), in EA.hy926 cells treated with DOX and PTUPB compared with human endothelial cells treated with DOX only. The protective effect of PTUPB against DOX-induced EndMT was further supported by a significant decrease in the ratio of mesenchymal cells to endothelial cells in DOX-incubated cells (Fig. 2I) and an improvement in the endothelial intracellular gap (Fig. 2J). Collectively, the findings of the present study demonstrated that PTUPB decreased DOX-induced EndMT.

Inhibition of sEH and COX-2 using PTUPB prevents DOX-induced endothelial and vascular dysfunction in zebrafish. Since PTUPB was shown to reduce DOX-induced EndMT in human endothelial cells *in vitro*, further tests were conducted to determine whether PTUPB was also able to protect against DOX-induced endothelial and vascular dysfunction *in vivo* in a zebrafish model of DOX-induced cardiovascular toxicity (Fig. 3A). Zebrafish were treated with DOX and/or PTUPB at 24 hpf (Fig. 3A). Viewpoints MicroZebralab software was used to assess the vascular function of zebrafish larvae at 72 hpf. DOX significantly reduced the blood velocity, diameter, and shear stress of the dorsal aorta (DA) and posterior cardinal vein (PCV) in zebrafish compared with those in the control group (Fig. 3B-H). However, the zebrafish group treated with DOX and PTUPB displayed significant improvements in blood velocity, diameter, and shear stress of the DA and PCV compared with those of zebrafish treated with DOX alone (Fig. 3B-H). Using RT-qPCR, the levels of EndMT markers in zebrafish were measured to assess whether PTUPB had any protective effect against DOX-induced endothelium damage. The results showed that DOX-incubated zebrafish exhibited

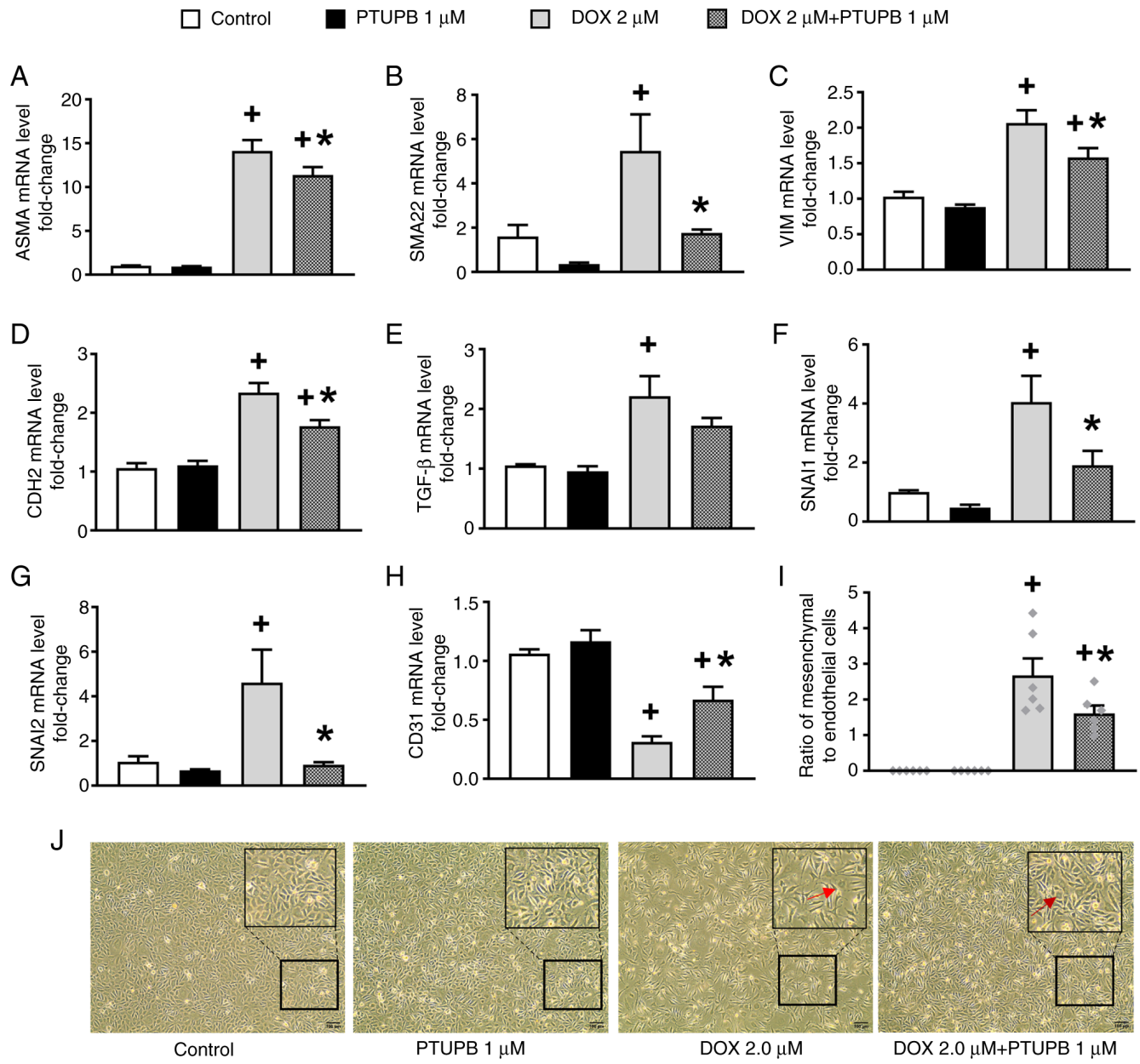

Figure 2. Inhibition of soluble epoxide hydrolase and cyclooxygenase-2 using PTUPB attenuates DOX-induced endothelial-to-mesenchymal transition. EA.hy926 cells were treated with 2 μM DOX with or without 1 μM PTUPB for 24 h. Gene expression levels of mesenchymal markers (A) ASMA, (B) SMA22, (C) VIM, (D) CDH2, (E) TGF-β, (F) SNAI1 and (G) SNAI2, and (H) endothelial marker CD31. (I) Ratio of mesenchymal to endothelial cells in cells treated with DOX with or without 1 μM PTUPB was measured based on morphological images. (J) Representative morphological images of EA.hy926 cells incubated with DOX with or without 1 μM PTUPB for 24 h at a magnification of x10 (scale bar, 100 μm). The light red arrow indicates mesenchymal cells (long, spindle-like cells). The dark red arrow indicates endothelial cells (cobblestone monolayer-like cells). One-way ANOVA followed by Tukey's multiple comparison test was performed to determine the significant differences between groups ($^{+}$P<0.05 vs. control, *P<0.05 vs. DOX). PTUPB, 4-[5-phenyl-3-[3-[[[[4-(trifluoromethyl)phenyl]amino]carbonyl]amino]propyl]-1H-pyrazol-1-yl]-benzenesulfonamide; DOX, doxorubicin; ASMA, smooth muscle actin α2; SMA22, smooth muscle protein 22α; VIM, vimentin; CDH2, cadherin-2; SNAI1, snail family transcriptional repressor 1; SNAI2, snail family transcriptional repressor 2.

a significant increase in systemic EndMT-related markers, including collagen 1a1 (col1a1; Fig. 3J), vim (Fig. 3K), tgf-β (Fig. 3L), and smooth muscle actin α2 (acta2; Fig. 3M), compared with the control group. On the other hand, PTUPB administered in conjunction with DOX significantly reduced the expression levels of EndMT markers, including col1a1 (Fig. 3J), vim (Fig. 3K), tgf-β (Fig. 3L), and acta2 (Fig. 3M), and significantly upregulated the levels of the systemic endothelial-related marker vegfr, compared with those of the zebrafish group treated with DOX alone (Fig. 3N). However, no significant changes in sna1 expression were observed in zebrafish treated with DOX and/or PTUPB (Fig. 3I). Together, the present data indicated that PTUPB protected against DOX-induced endothelial and vascular toxicity in zebrafish.

Inhibition of sEH and COX-2 using PTUPB prevents DOX-induced cardiac dysfunction in zebrafish. While the protective effect of PTUPB on the pathogenesis of DOX-induced endothelial and vascular toxicity was demonstrated, the present

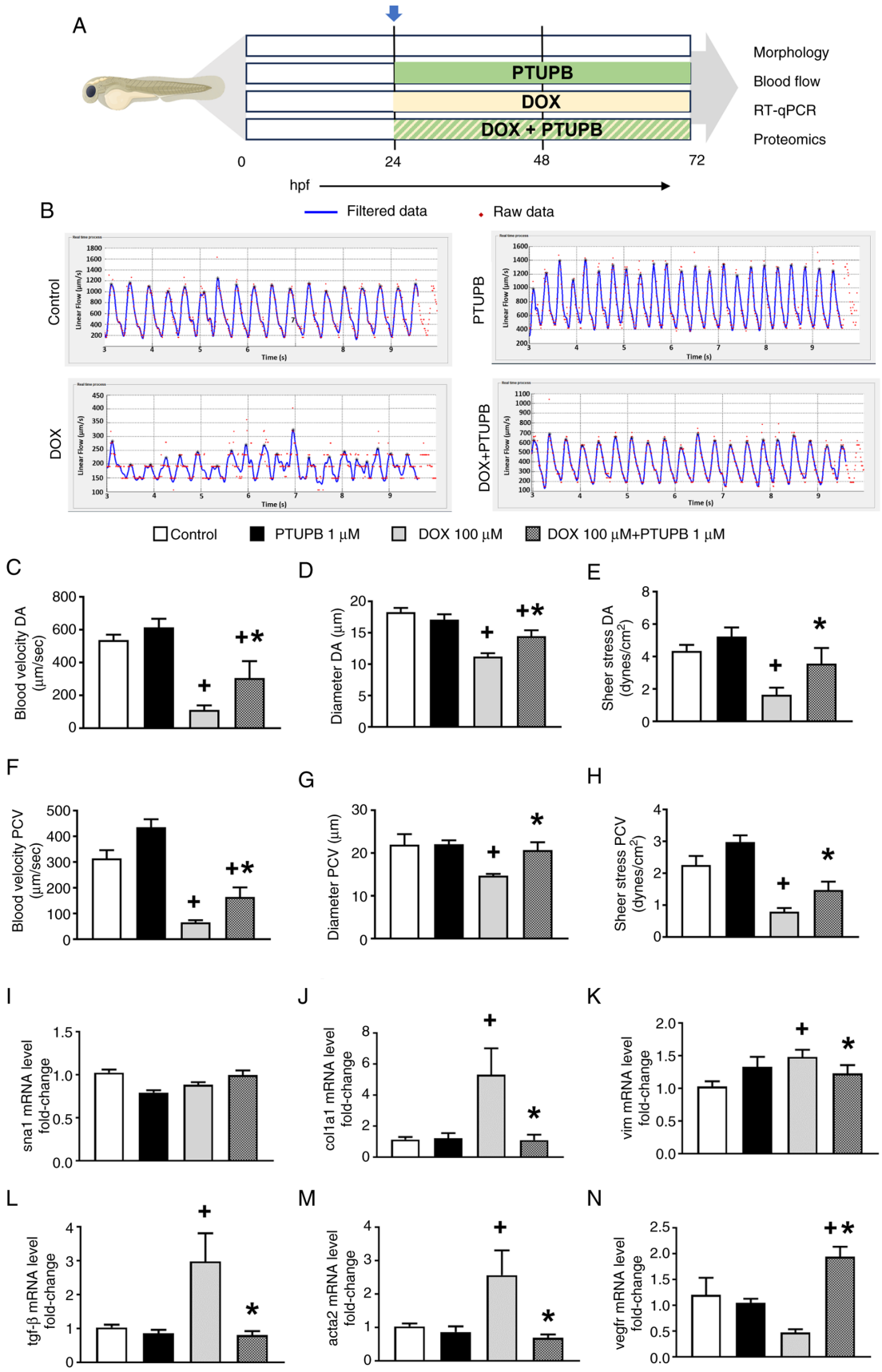

Figure 3. PTUPB prevents DOX-induced endothelial and vascular dysfunction in zebrafish. (A) Schematic representation of the treatment protocol in zebrafish. Zebrafish embryos were treated at 24 hpf with 100 μM DOX with or without 1 μM PTUPB for 48 h. (B) Representative images of velocity-time integral graphs obtained from the MicroZebralab software for the DA and PCV of zebrafish at 72 hpf. (C and F) Blood velocity, (D and G) diameter and (E and H) shear stress of the (C-E) DA and (F-H) PCV. Gene expression levels of (I) sna1, (J) col1a1, (K) vim, (L) tgf-β, (M) acta2 and (N) vegfr. $^{+}$P<0.05 vs. control, *P<0.05 vs. DOX). DOX, doxorubicin; PTUPB, 4-[5-phenyl-3-[3-[[[[4-(trifluoromethyl)phenyl]amino]carbonyl]amino]propyl]-1H-pyrazol-1-yl]-benzenesulfonamide; hpf, hours post-fertilization; RT-q, reverse transcription-quantitative PCR; DA, dorsal aorta; PCV, posterior cardinal vein; sna1, snail family zinc finger 1a; col1a1, collagen 1a1; vim, vimentin; acta2, smooth muscle actin α2.

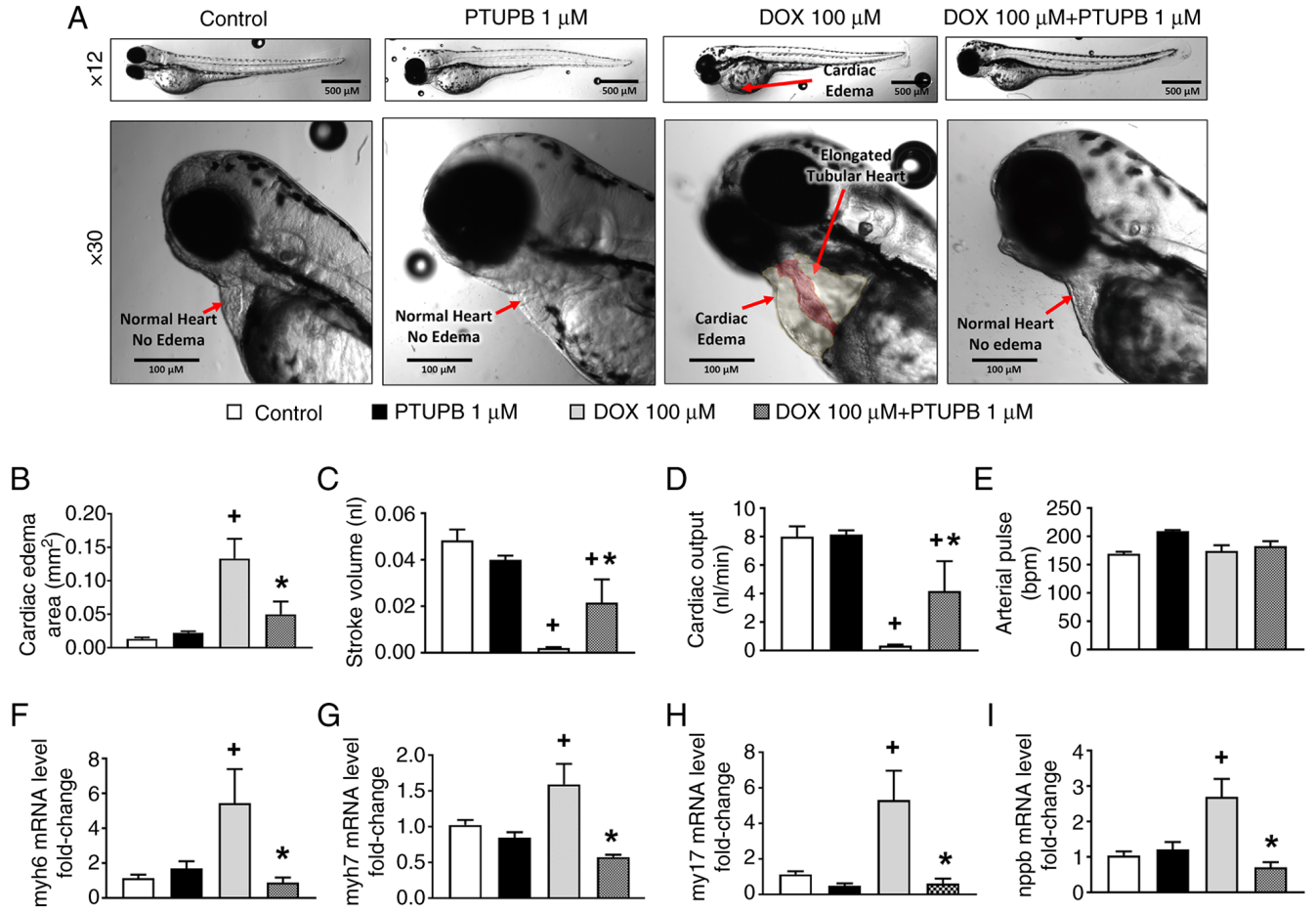

Figure 4. PTUPB prevents DOX-induced cardiac dysfunction in zebrafish. (A) Representative images of cardiac morphology in zebrafish larvae at 72 h post-fertilization. (B) Cross-sectional area of cardiac edema in mm^2. (C) Stroke volume, (D) cardiac output and (E) arterial pulse in zebrafish larvae treated with DOX and PTUPB. Gene expression levels of zebrafish cardiac injury markers (F) myh6, (G) myh7, (H) myl7 and (I) nppb. One-way ANOVA followed by Tukey's multiple comparison test was performed to determine the significant differences between groups ($^{+}P<0.05$ vs. control, $^{*}P<0.05$ vs. DOX). DOX, doxorubicin; PTUPB, 4-[5-phenyl-3-[3-[[[[4-(trifluoromethyl)phenyl]amino]carbonyl]amino]propyl]-1H-pyrazol-1-yl]-benzenesulfonamide; myh6, myosin heavy chain 6; myh7, myosin heavy chain 7; myl7, myosin light chain 7; nppb, natriuretic peptide B.

study also aimed to investigate whether PTUPB could reduce DOX-induced cardiac dysfunction. To do this, the cardiac structure and function, as well as systemic cardiac toxicity-related markers, were examined in zebrafish incubated with DOX. DOX-treated zebrafish exhibited a significant increase in cardiac edema (Fig. 4A and B), a significant decrease in stroke volume (Fig. 4C) and cardiac output (Fig. 4D), as well as significant upregulation of the systemic cardiotoxicity-related markers myosin heavy chain 6 (myh6; Fig. 4F), myosin heavy chain 7 (myh7; Fig. 4G), myosin light chain 7 (myl7; Fig. 4H) and natriuretic peptide B (nppb; Fig. 4I) when compared with the control group. Notably, PTUPB was observed to significantly reduce cardiac edema (Fig. 4A and B) and significantly improve stroke volume (Fig. 4C) and cardiac output (Fig. 4D) in DOX-treated zebrafish. The cardioprotective effect of PTUPB was further supported by the significant downregulation of systemic cardiotoxicity-related markers, including myh6 (Fig. 4F), myh7 (Fig. 4G), myl7 (Fig. 4H), and nppb (Fig. 4I), in zebrafish administered PTUPB and DOX together compared with DOX-treated zebrafish. However, no significant changes in arterial pulse were observed in zebrafish treated with DOX and/or PTUPB (Fig. 4E). Overall, the present data provided evidence that PTUPB improved cardiovascular function in DOX-treated zebrafish.

Protective effects of PTUPB against DOX-induced endothelial, vascular and cardiac toxicity are associated with the suppression of systemic inflammation, oxidative stress and apoptosis. Since inflammation, oxidative stress and apoptosis are known mediators of EndMT, as well as endothelial, vascular and cardiac toxicity, and previous reports have demonstrated that the inhibition of sEH and COX-2 using PTUPB reduced inflammation and vascular endothelial injury (23,44,46,47), it was hypothesized that PTUPB may reduce inflammation, oxidative stress and apoptosis, and mitigate DOX-induced vascular endothelial and cardiac toxicity. To test this, the effect of PTUPB on systemic inflammation, oxidative stress, and apoptosis-related markers was examined in zebrafish treated with DOX. Zebrafish administered DOX, when compared with the control group, displayed significant upregulation of: i) Systemic inflammation-related markers il-1b (Fig. 5A), tnfα (Fig. 5B), nfκb (Fig. 5C) and il-10 (Fig. 5D); ii) systemic oxidative stress-related markers glutathione peroxidase (gpx; Fig. 5E), catalase (cat; Fig. 5F), heme oxygenase 1a (hmox; Fig. 5G) and NAD(P)H dehydrogenase quinone 1 (nqo1; Fig. 5H); and iii) systemic apoptosis-related markers bax (Fig. 5I), caspase-3 (Fig. 5K) and caspase-7 (Fig. 5L). The data suggested that inflammation, oxidative stress and apoptosis

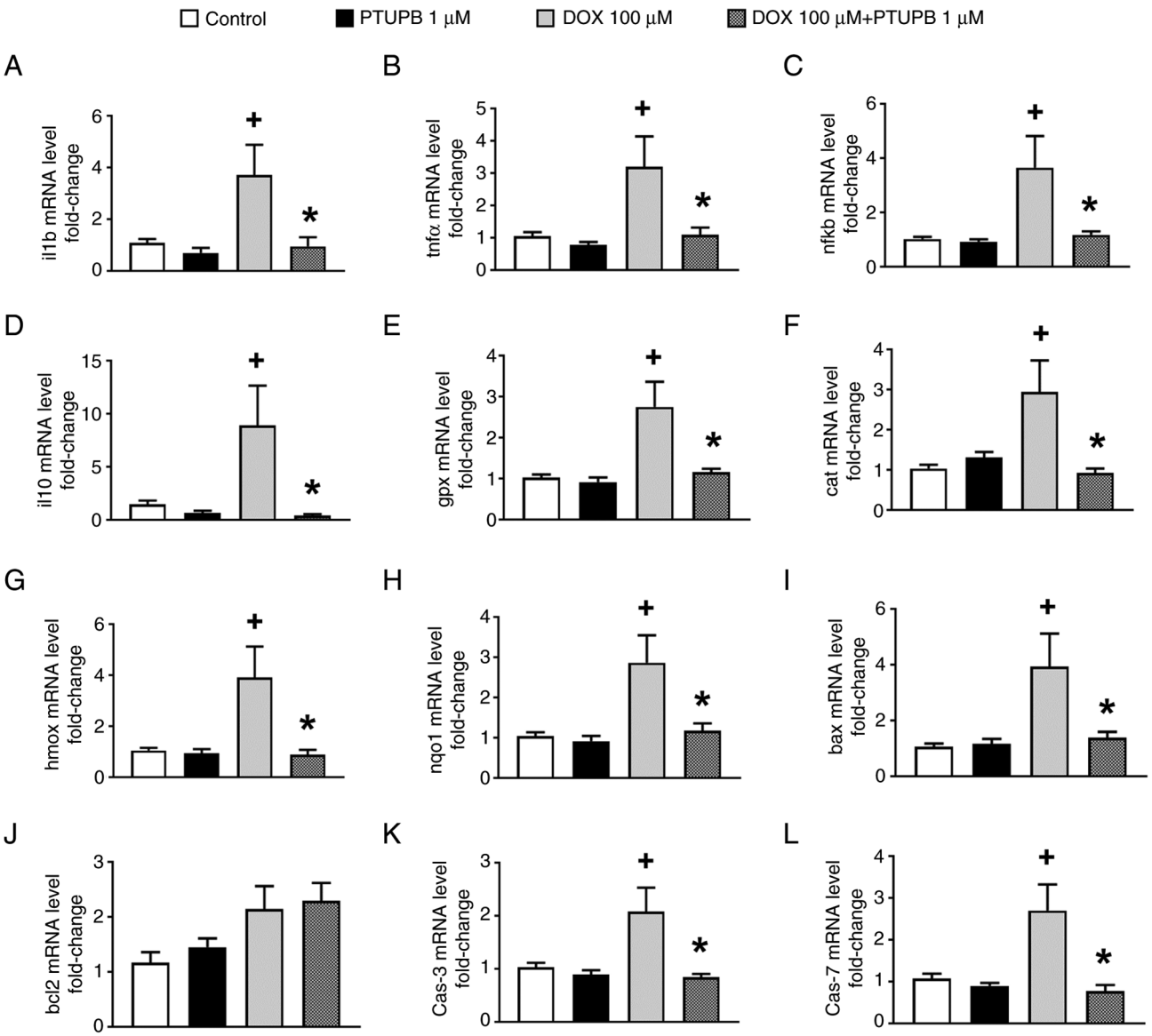

Figure 5. PTUPB reduces DOX-induced inflammation, oxidative stress and apoptosis. Gene expression levels of zebrafish inflammatory markers (A) il1b, (B) tnfα, (C) nfκb and (D) il10, oxidative stress markers (E) gpx, (F) cat, (G) hmox and (H) nqo1, and apoptosis markers (I) bax, (J) bcl2, (K) cas-3 and (L) cas-7. One-way ANOVA followed by Tukey's multiple comparison test was performed. $^{+}$P<0.05 vs. control, *P<0.05 vs. DOX). DOX, doxorubicin; PTUPB, 4-[5-phenyl-3-[3-[[[[4-(trifluoromethyl)phenyl]amino]carbonyl]amino]propyl]-1H-pyrazol-1-yl]-benzenesulfonamide; gpx, glutathione peroxidase; cat, catalase; hmox, heme oxygenase 1a; nqo1, NAD(P)H dehydrogenase quinone 1; cas-3, caspase 3; cas-7, caspase 7.

were implicated in DOX-induced endothelial, vascular and cardiac toxicity (Fig. 5). Consistent with the present hypothesis, PTUPB administration in DOX-treated zebrafish, when compared with zebrafish treated only with DOX, significantly reduced the upregulation of: i) Systemic inflammation-related markers il-1b (Fig. 5A), tnfα (Fig. 5B), nfκb (Fig. 5C) and il-10 (Fig. 5D); ii) systemic oxidative stress-related markers gpx (Fig. 5E), cat (Fig. 5F), hmox (Fig. 5G) and nqo1 (Fig. 5H); and iii) systemic apoptosis-related markers bax (Fig. 5I), caspase-3 (Fig. 5K) and caspase-7 (Fig. 5L). However, no significant changes in bcl2 expression were observed in the zebrafish treated with DOX and/or PTUPB (Fig. 5J). Overall, these findings showed that the mitigating effects of PTUPB against DOX-induced vascular, endothelial, and cardiac toxicity were mediated by reducing inflammation, oxidative stress, and apoptosis.

Protective effects of PTUPB against DOX-induced endothelial, vascular and cardiac toxicity are associated with the alteration of the systemic zebrafish proteomics profile. To test the effect of PTUPB on DOX-induced cardiovascular toxicity at the proteome level, a proteomic profiling experiment was performed using zebrafish treated with control, DOX and/or PTUPB. Notably, a total of 898 proteins were detected using MaxQuant analysis in zebrafish (Fig. 6). While the expression levels of 49 proteins were significantly altered in zebrafish incubated with DOX compared with the control group (Fig. 6A), the combination of DOX and PTUPB significantly modulated 17 proteins compared with the DOX group (Fig. 6B).

The effects of DOX and PTUPB on proteins related to EndMT and cardiotoxicity were further investigated in the zebrafish proteomic profile. Consistent with the present findings on mRNA expression and blood flow, the present

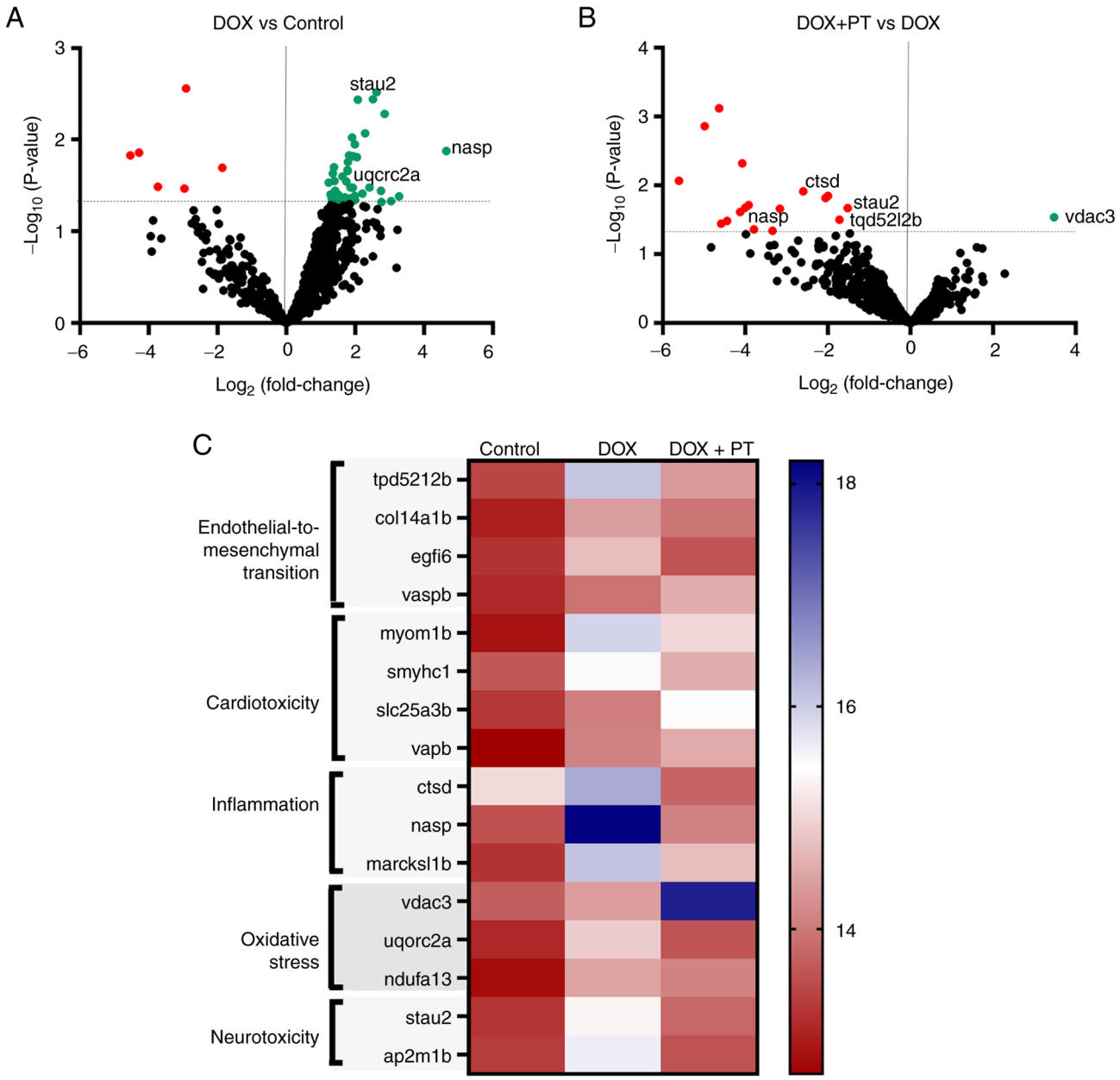

Figure 6. Impact of PTUPB on the proteomic profile of zebrafish treated with DOX. Volcano comparison plot of -$\log_{10}$ P-values vs. $\log_2$ fold change of differentially expressed proteins for (A) DOX vs. control and (B) DOX + PTUPB vs. DOX. (C) Heatmap of significant differential expression of proteins for control larvae, and zebrafish larvae treated with DOX alone or a combination of DOX and PTUPB. PTUPB, 4-[5-phenyl-3-[3-[[[[4-(trifluoromethyl)phenyl]amino] carbonyl]amino]propyl]-1H-pyrazol-1-yl]-benzenesulfonamide; DOX, doxorubicin.

study found that zebrafish administered with DOX displayed significant upregulation of EndMT-related protein expression, including tpd52 like 2b (tpd52l2b), collagen type XIV α1b (col14a1b) and egfl6 expression, and cardiotoxicity-related protein expression, including myomesin 1b (myom1b) and slow myosin heavy chain 1 (smyhc1) expression, compared with those in the control group (Table I; Fig. 6C). PTUPB significantly reduced the expression levels of the EndMT marker tpd52l2b, in zebrafish treated with DOX compared with DOX alone (Table I; Fig. 6C) and upregulated the expression levels of vascular endothelial protector protein, vasodilator-stimulated phosphoprotein b, and cardioprotective proteins, solute carrier family 25-member 3b and VAMP-associated protein B, in zebrafish-treated with DOX compared with control (Table I; Fig. 6C). Furthermore, there was no significant change in the expression levels of EndMT-related proteins, tpd52l2b, col14a1b and egfl6, and cardiotoxicity-related proteins, myom1b and smyhc1, in the DOX-PTUPB group compared with the control group (Table I; Fig. 6C). Overall, the present findings suggested that PTUPB mitigated the DOX-induced upregulation of EndMT- and cardiotoxicity-related proteins.

Given that inflammation and oxidative stress serve a detrimental role in DOX-induced cardiovascular toxicity, the present study examined the effect of DOX and PTUPB on proteins related to inflammation and oxidative stress in the zebrafish proteomic profile. Notably, zebrafish administered with DOX displayed significant upregulation of inflammation-related proteins, nuclear autoantigenic sperm protein (nasp),

Table I. Protein expression profile of zebrafish embryos treated with DOX and DOX + PTUPB.

A, Endothelial-to-mesenchymal transition

		DOX vs. control		DOX + PTUPB vs. DOX		DOX + PTUPB vs. control	
Protein ID	Protein name	Log_2 fold change	P-value	Log_2 fold change	P-value	Log_2 fold change	P-value
A0A8M9PWB5	Tpd52 like 2b	2.636	0.003	-1.722	0.032	0.914	0.220
A0A8M9PS14	Collagen, type XIV, α1b	1.381	0.020	-0.432	0.417	0.949	0.090
A0A8M6Z078	EGF-like-domain, multiple 6	1.507	0.041	-1.138	0.109	0.369	0.584
Q1LVK6	Vasodilator-stimulated phosphoprotein b	0.827	0.192	0.607	0.331	1.433	0.034

B, Cardiotoxicity markers

		DOX vs. control		DOX + PTUPB vs. DOX		DOX + PTUPB vs. control	
Protein ID	Protein name	Log_2 fold change	P-value	Log_2 fold change	P-value	Log_2 fold change	P-value
A0A8M6Z7G3	Myomesin 1b	3.043	0.047	-0.921	0.514	2.123	0.148
A0A0R4INI3	Slow myosin heavy chain 1	1.865	0.043	-0.940	0.277	0.926	0.284
Q7ZV45	Solute carrier family 25-member 3b	0.761	0.462	1.435	0.178	2.197	0.049
Q6P2B0	VAMP-associated protein B	1.401	0.054	0.431	0.521	1.833	0.016

C, Inflammation

		DOX vs. control		DOX + PTUPB vs. DOX		DOX + PTUPB vs. control	
Protein ID	Protein name	Log_2 fold change	P-value	Log_2 fold change	P-value	Log_2 fold change	P-value
Q8AWD9	Cathepsin D	1.327	0.157	-2.590	0.012	-1.268	0.174
F1QNE0	Nuclear autoanti-genic sperm protein	4.653	0.013	-4.125	0.024	0.528	0.747
Q6NWH2	MARCKS-like 1b	2.853	0.005	-1.367	0.127	1.486	0.100

D, Oxidative stress

		DOX vs. control		DOX + PTUPB vs. DOX		DOX + PTUPB vs. control	
Protein ID	Protein name	Log_2 fold change	P-value	Log_2 fold change	P-value	Log_2 fold change	P-value
A0A8M2BEA2	Voltage-dependent anion channel 3	0.675	0.639	3.481	0.029	4.156	0.012
F1QJE0	Ubiquinol-cytochrome *c* reductase core protein 2a	1.779	0.047	-1.293	0.339	0.486	0.555
Q6PC49	NADH:ubiquinone oxidoreductase subunit A13	1.629	0.025	-0.340	0.602	1.289	0.066

Table I. Continued.

E, Neurotoxicity markers

		DOX vs. control		DOX + PTUPB vs. DOX		DOX + PTUPB vs. control	
Protein ID	Protein name	Log_2 fold change	P-value	Log_2 fold change	P-value	Log_2 fold change	P-value
Q7ZW47	Staufen double-stranded RNA binding protein 2	2.077	0.004	-1.521	0.021	0.556	0.352
Q7ZW98	Adaptor-related protein complex 2 subunit mu 1b	2.291	0.009	-2.060	0.015	0.231	0.756

DOX, doxorubicin; PTUPB, 4-[5-phenyl-3-[3-[[[[4-(trifluoromethyl)phenyl]amino]carbonyl]amino]propyl]-1H-pyrazol-1-yl]-benzenesulfonamide.

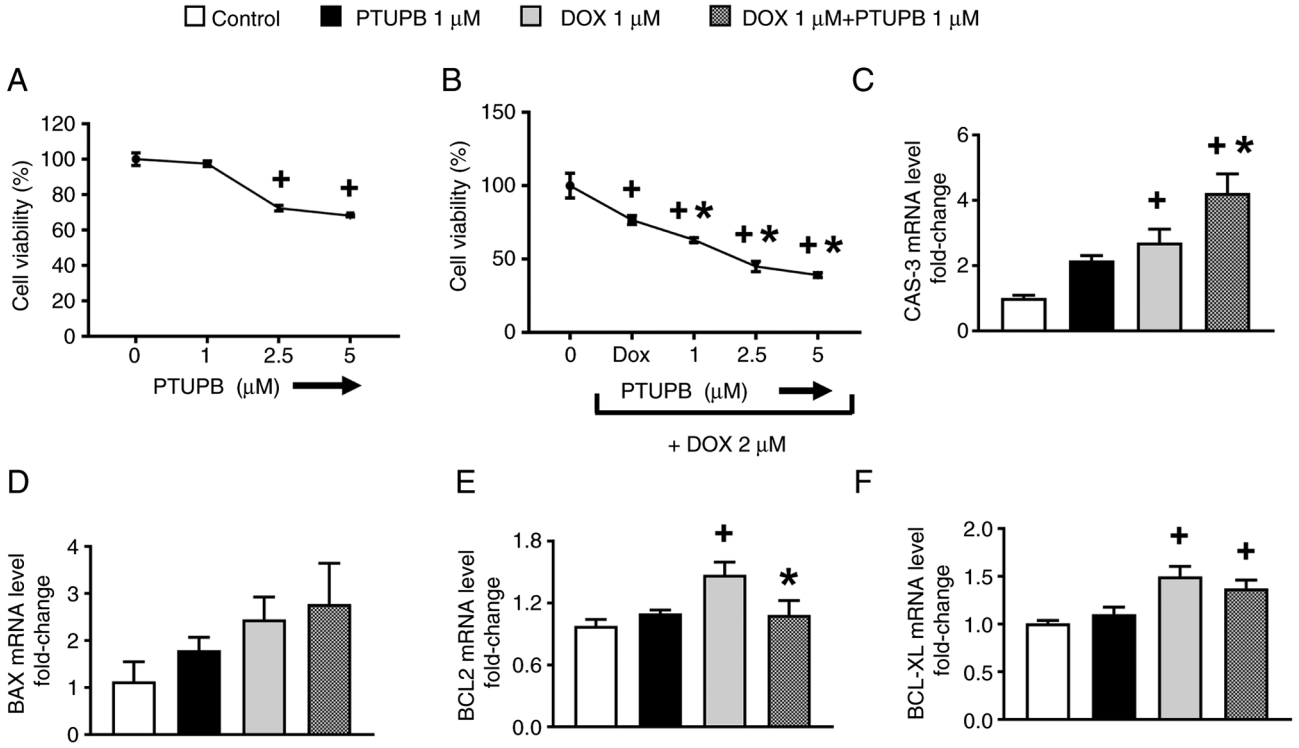

Figure 7. PTUPB does not negate the anticancer effect of DOX in human breast cancer cells. Viability of MDA-MB-231 cells treated with (A) PTUPB alone or (B) DOX with PTUPB. MDA-MB-231 cells were treated with 2 μM DOX alone or in combination with 1 μM PTUPB for 24 h. Gene expression levels of apoptotic markers (C) CAS-3, (D) BAX, (E) BCL2 and (F) BCL-XL. One-way ANOVA followed by Tukey's multiple comparison test was performed to determine the significant difference between groups ($^{+}$P<0.05 vs. control, *P<0.05 vs. DOX). DOX, doxorubicin; PTUPB, 4-[5-phenyl-3-[3-[[[[4-(trifluoromethyl)phenyl]amino]carbonyl]amino]propyl]-1H-pyrazol-1-yl]-benzenesulfonamide; Cas-3, caspase-3.

MARCKS-like 1b (marcksl1b), and oxidative stress-related proteins, ubiquinol-cytochrome *c* reductase core protein 2a (uqcrc2a) and NADH:ubiquinone oxidoreductase subunit A13 (ndufa13), compared with those in the control group (Table I; Fig. 6C). On the other hand, PTUPB significantly downregulated the expression levels of inflammation-related proteins, nasp and cathepsin D, in DOX-treated zebrafish compared with zebrafish treated with DOX alone (Table I; Fig. 6C). PTUPB significantly upregulated the expression levels of the antioxidant protein voltage-dependent anion channel 3 in DOX-treated zebrafish compared with zebrafish treated with DOX alone and the control group (Table I; Fig. 6C). However, there was no significant change in the expression levels of inflammation-related proteins, nasp, marcksl1b , and oxidative stress-related proteins, uqcrc2a and ndufa13, in the DOX-PTUPB group compared with the control group (Table I; Fig. 6C). Collectively, the aforementioned findings suggested that PTUPB reduced DOX-induced inflammation and oxidative stress at the proteome level.

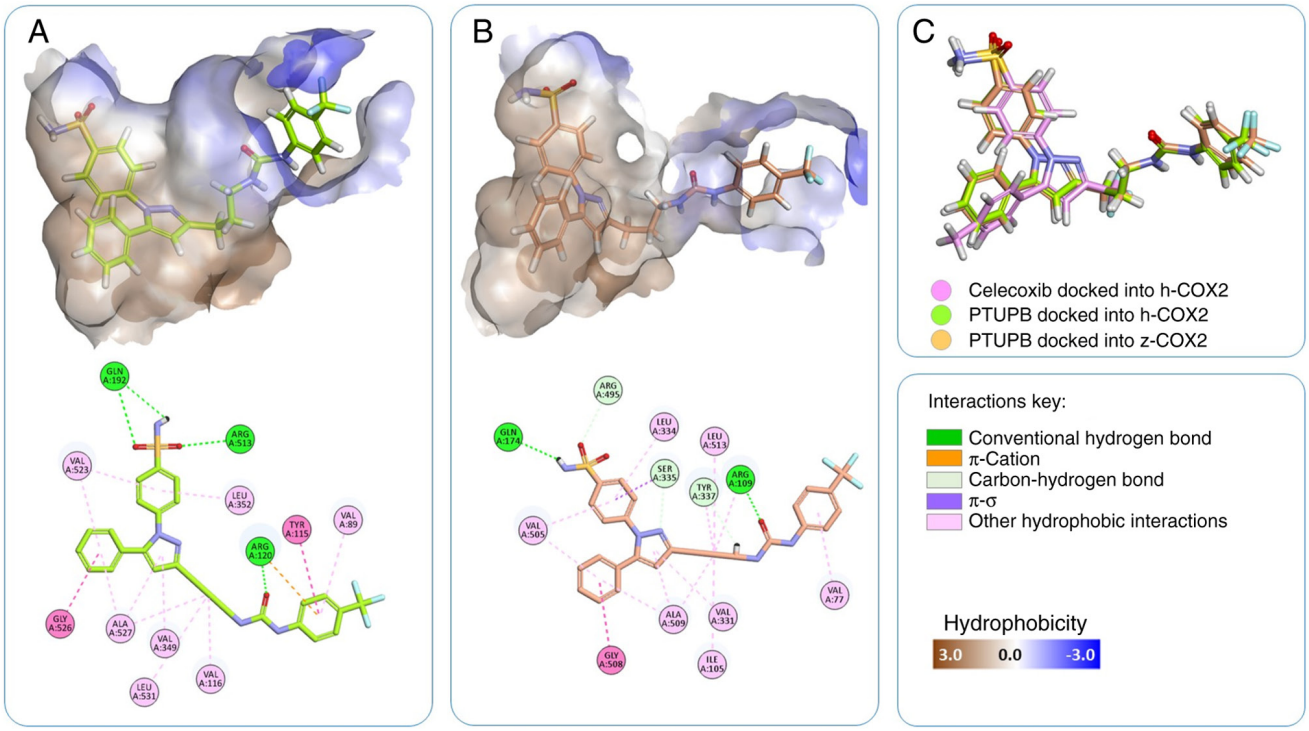

Figure 8. Binding modes of docked PTUPB within the active sites of the h- and z-COX-2 isoforms. (A) h-COX-2-PTUPB complex. (B) z-COX-2-PTUPB complex. In each panel, there is a 3D surface representation of the binding site along with a 2D interaction map. The surface is colored according to hydrophobicity, and the interacting amino acids are colored according to the type of intermolecular interaction they are involved in. (C) Superimposition of PTUPB in each complex and binding orientation of celecoxib. PTUPB, 4-[5-phenyl-3-[3-[[[[4-(trifluoromethyl)phenyl]amino]carbonyl]amino]propyl]-1H-pyrazol-1-yl]-benzenesulfonamide; COX-2, cyclooxygenase-2; h-, human; z-, zebrafish.

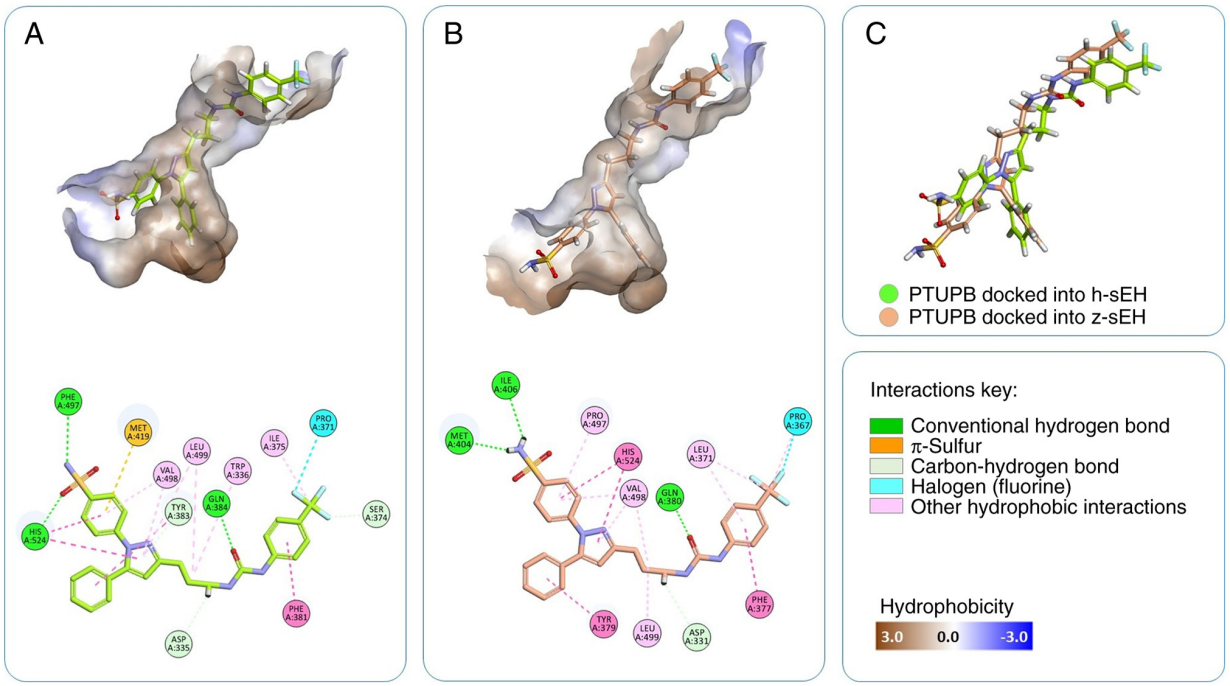

Figure 9. Binding modes of docked PTUPB within the active sites of the h- and z-sEH isoforms. (A) h-sEH-PTUPB complex. (B) z-sEH-PTUPB complex. (C) Superimposition of PTUPB in (A and B). PTUPB, 4-[5-phenyl-3-[3-[[[[4-(trifluoromethyl)phenyl]amino]carbonyl]amino]propyl]-1H-pyrazol-1-yl]-benzenesulfonamide; sEH, soluble epoxide hydrolase; h-, human; z-, zebrafish.

Another important finding in the zebrafish proteomic profile was that zebrafish administered DOX displayed significant upregulation of memory and cognitive function-related proteins, such as staufen double-stranded RNA binding protein 2 and adaptor-related protein complex 2 subunit mu 1b, compared with the control group (Table I; Fig. 6C). On the

Table II. Predicted binding affinities of PTUPB for the proteins based on CDOCKER scores in kcal/mol.

Compound	h-COX-2	z-COX-2	h-sEH	z-sEH	Comments
Rofecoxib	-48.46	-	-	-	Co-crystallized inhibitor of h-COX-2 (PDB ID 5KIR); redocked as a docking validation step
Celecoxib	-50.48	-39.64	-	-	Docked into the rofecoxib binding site
K78	-	-	-56.42	-	Co-crystallized inhibitor of h-sEH (PDB ID 5AI9); redocked as a docking validation step
t-AUCB	-	-	-51.33	-44.50	Known inhibitor of h-sEH
PTUPB	-58.10	-34.03	-56.30	-43.88	Reference compound

h-COX-2, human cyclooxygenase-2; z-COX-2, zebrafish cyclooxygenase-2; t-AUCB, 4-[[trans-4-[[(tricyclo[3.3.1.13,7]dec-1-ylamino) carbonyl]amino]cyclohexyl]oxy]-benzoic acid; PTUPBP, 4-[5-phenyl-3-[3-[[[[4-(trifluoromethyl)phenyl]amino]carbonyl]amino]propyl]-1H-pyrazol-1-yl]-benzenesulfonamide; celecoxib, 4-[5-(4-methylphenyl)-3-(trifluoromethyl)-1H-pyrazol-1-yl]-benzenesulfonamide; h-sEH, human soluble epoxide hydrolase; z-sEH, zebrafish soluble epoxide hydrolase; PDB, Protein Data Bank.

other hand, PTUPB significantly reduced the expression levels of these proteins in DOX-treated zebrafish compared with zebrafish treated with DOX alone (Table I; Fig. 6C). These findings suggested that PTUPB may also improve the neuronal function of DOX-treated zebrafish. Further investigations are needed to confirm these findings.

PTUPB does not negate the anticancer effect of DOX in breast cancer cells. Given that the purpose of the present study was to reduce the adverse effect of DOX without compromising its anticancer activity, the impact of PTUPB on the anticancer effect of DOX was tested in the MDA-MB-231 triple-negative breast cancer cell line. To achieve this, MDA-MB-231 cells were incubated with increasing concentrations of PTUPB either alone or with 2 μM DOX. PTUPB (2.5 and 5 μM significantly decreased the viability of MDA-MB-231 cells compared to the control group (Fig. 7A). Notably, PTUPB reduced the cell viability in the DOX-treated group compared with the control group in a concentration-dependent manner (Fig. 7B). Additionally, while PTUPB did not significantly affect bax and B-cell lymphoma extra-large expression (Fig. 7D and F), PTUPB further upregulated DOX-induced caspase-3 expression (Fig. 7C) and significantly reduced DOX-induced bcl2 expression (Fig. 7E) compared with the DOX treatment group. Overall, the present data indicated that PTUPB potentiated the anticancer effect of DOX in human triple-negative breast cancer cells.

Computational investigation of the binding affinity of PTUPB towards both human and zebrafish isoforms of the sEH and COX-2 enzymes. In the present study, the biological effects of the compound PTUPB might be attributed to its inhibitory activity against the COX-2 and sEH enzymes. The experimental investigations and their corresponding results were obtained based on zebrafish models and, to a lesser extent, human epithelial cells, as in a previous study (48). Therefore, computational methods were employed to investigate the binding affinity of PTUPB towards both the human and zebrafish isoforms of the two proteins, as will be discussed in the following paragraphs and demonstrated in (Figs. 8 and 9) and Table II. This computational study was intended to validate the transferability and applicability of the experimental results obtained from zebrafish models to human biological settings. Due to the structural and sequence similarities between human COX-1 and COX-2 isoforms, the selectivity of PTUPB towards COX-2 vs. COX-1 was investigated by docking PTUPB into the human COX-1 enzyme.

Protein sequences of human sEH (h-sEH) and COX-2 are similar to those found in zebrafish. When proteins share high sequence identity and sequence similarity, this implies that their 3D structure and binding sites are also likely to show high similarity. Hence, the ligand-binding interactions of one isoform can be extrapolated to the other isoform with reasonable confidence (49-51). The sequence alignment of the full-length COX-2 and sEH proteins of the two species, zebrafish and human, showed 67.00 and 49.30% sequence identity and 85.00 and 71.60% sequence similarity between the respective protein isoforms of the two species (Fig. S2). Furthermore, sEH is a homodimer protein in which each monomer is composed of two domains, the 35-kDa C-terminal domain and the 25-kDa N-terminal domain, with the former being responsible for the catalytic activity of the enzyme (52). In the present study, the C-terminal domain was utilized for docking studies. Notably, the catalytic C-terminal domain of sEH shared a higher sequence identity (61.0%) and similarity (78.6%) between the two species compared with the full-length protein, making predictions based on docking results using this domain more accurate. The sequence alignment of the z-COX-2 and human COX-2 (h-COX-2) enzymes, as shown in Fig. S2, revealed that the main amino acid residues involved in catalysis or ligand binding were conserved in both isoforms, namely (as per h-COX-2 numbering) Arg120, Tyr348, Val349, Tyr385, Trp387, Val434, and Val523. For sEH, the main amino acid residues involved in catalysis were Asp335, Asp496, and His524, while in substrate binding, they were Tyr466, Trp336, Tyr383, and Gln384.

Docking validation. Following sequence alignments, the docking study commenced. Firstly, the co-crystallized ligands

were extracted and redocked into their respective binding sites. This was performed as a docking validation step, and the docking algorithm was successful at regenerating the native co-crystallized poses (Fig. S3) with a root mean square deviation (RMSD) of the redocked ligands into COX-2 and sEH from their native congeners of 0.50 and 0.48 Å, respectively. RMSD values <2 Å were acceptable, with lower values indicating more favorable docking scores (53). Since the 4-(5-phenyl-1H-pyrazol-1-yl)benzenesulfonamide section of PTUPB is identical to that of celecoxib (Fig. S1), the latter was also docked into the binding sites of the two species of COX-2 isoforms for comparison purposes regarding its binding orientation.

Predicted binding affinity of PTUPB for human and zebrafish sEH and COX-2. Following the docking validation step, PTUPB was docked into the binding sites of the two isoforms of the human and zebrafish sEH and COX-2 enzymes. Table II shows the predicted binding affinity of PTUPB for all proteins. The docking scores presented in Table II show that the predicted binding affinity of PTUPB for h-COX-2 (-58.10 kcal/mol) was comparable with that of celecoxib and rofecoxib, selective COX-2 inhibitors with binding affinities of -50.48 and -48.46 kcal/mol, respectively, supporting the potential inhibitory effect of PTUPB against h-COX-2. PTUPB also demonstrated a notable binding affinity towards z-COX-2, with a predicted binding affinity of -34.03 kcal/mol compared with -39.64 kcal/mol for celecoxib. These comparisons implied that PTUPB was likely to be a dual inhibitor of h-COX-2 and z-COX-2. To assess the selectivity of PTUPB against human COX isozymes, it was docked into the human COX-1 enzyme. However, it failed to dock, suggesting that PTUPB could be a selective COX-2 inhibitor, which is a desirable property that would translate into fewer side effects compared with non-selective analogs. This isozyme selectivity was expected due to the high structural identity of the 4-(5-phenyl-1H-pyrazol-1-yl)benzenesulfonamide segment of PTUPB with celecoxib and the topological differences between the binding sites of both COX isozymes. Celecoxib is a selective COX-2 inhibitor because it cannot fit the smaller allosteric pocket in the COX-1 enzyme (54).

Similar to its notable binding affinity towards COX-2 isoforms, PTUPB also showed marked binding affinities towards human and zebrafish sEH isoforms, which supported its potential dual inhibitory effect against COX-2 and sEH enzymes. PTUPB showed comparable predicted binding affinity (-56.30 kcal/mol) to that of the co-crystallized K78 inhibitor (-56.42 kcal/mol) and a stronger binding affinity compared with the h-sEH inhibitor t-AUCB (-51.33 kcal/mol) towards the h-sEH enzyme. Similar results were obtained for the PTUPB binding affinity for zebrafish sEH (-43.88 kcal/mol) compared with that of t-AUCB (-44.50 kcal/mol). A notable observation in these results was that the docking scores of PTUPB for the zebrafish enzymes (COX-2 and sEH) were lower than those for their human counterparts (Table II).

Molecular docking of PTUPB into the binding sites of human and zebrafish sEH and COX-2. In addition to the docking scores, the binding modes and interactions of PTUPB within the binding sites of target proteins should also be considered. Figs. 8 and 9 show the 3D binding modes of PTUPB within the binding sites of the isoforms of h- and z-COX-2 and sEH proteins, along with their respective 2D interaction maps. Figs. 8 and 9 show that PTUPB adopted the same 3D binding orientation within each set of enzyme isoforms. Furthermore, PTUPB established similar types of intermolecular interactions with conserved amino acid residues as inferred from the respective 2D interaction maps. PTUPB established effective interactions with key amino acid residues within h-COX-2, such as hydrogen bond (H-bond) interaction with Arg120, and hydrophobic interactions with Val349 and Val523. Similarly, PTUPB interactions within the z-COX-2 involved H-bonding with Arg109, and hydrophobic interactions with Val331 and Val505 (key amino acid counterparts of those in h-COX-2). For PTUPB interactions with the h-sEH, it established a carbon-hydrogen bond with Asp335 (Asp331 in z-sEH), H-bond and hydrophobic interactions with His524 (His524 in z-sEH), hydrophobic interactions with Trp336 (Trp331 in z-sEH), Tyr383 (Tyr379 in z-sEH) and H-bond with Gln384 (Gln380 in z-sEH). Based on the aforementioned computational results, PTUPB bound effectively to h-COX-2 and h-sEH in a similar manner to z-COX-2 and z-sEH but with a higher binding affinity. Additionally, the binding affinities of PTUPB toward sEH were stronger than those toward COX-2 in zebrafish.

PTUPB exhibits a cardioprotective effect in the zebrafish model of DOX-induced cardiovascular toxicity, likely through the inhibition of sEH. Given that PTUPB has a preferential inhibitory effect on sEH compared with COX-2, based on the aforementioned drug docking findings and as described previously (48), we hypothesized that the protective effect of PTUPB on DOX-induced cardiovascular toxicity was likely to be attributed to the inhibition of sEH. The present study predicted that a selective inhibitor of sEH, such as t-AUCB, would exert beneficial effects on DOX-induced cardiovascular toxicity similar to those observed for PTUPB (Figs. 3 and 4). To test this hypothesis, zebrafish were treated with control, t-AUCB alone, DOX alone, or a combination of DOX and t-AUCB at 24 hpf (Fig. 10A). Viewpoints MicroZebralab software was used to assess the cardiac and vascular function of zebrafish larvae at 72 hpf. Notably, in a manner similar to what was observed for PTUBP, t-AUCB significantly reduced cardiac edema (Fig. 10B and C) and improved the stroke volume and cardiac output (Fig. 10D and E) compared with those of zebrafish treated with DOX alone. However, no significant changes in arterial pulse were observed in zebrafish treated with DOX and/or t-AUCB (Fig. 4F). Besides the cardiac effects, the zebrafish group treated with DOX and t-AUCB exhibited significant improvements in blood velocity and the diameter of the DA and PCV compared with zebrafish treated with DOX alone (Fig. 10G-J). Overall, the data indicated that the inhibition of sEH by t-AUCB protected against DOX-induced cardiac and vascular toxicity in zebrafish.

Given that EETs are known targets of sEH inhibitors, the present study tested the hypothesis that blocking the formation of EETs would eliminate the beneficial effects of sEH inhibitors such as PTUPB. To test this hypothesis, zebrafish were treated with control, DOX alone, DOX + PTUPB, or a combination of DOX, PTUPB, and EET formation inhibitor,

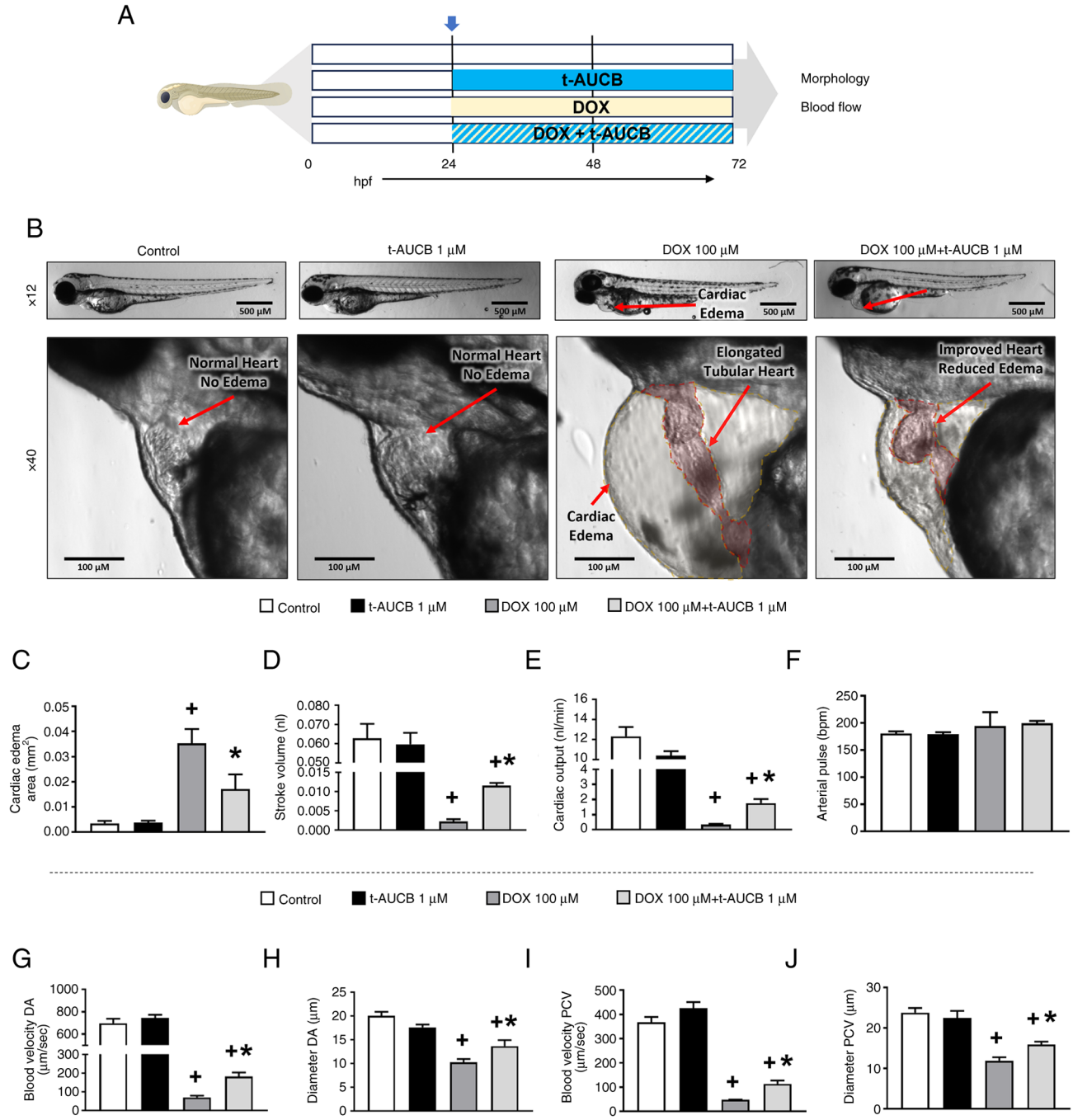

Figure 10. t-AUCB prevents DOX-induced cardiac and vascular dysfunction in zebrafish. (A) Schematic representation of the treatment protocol. (B) Representative images of cardiac morphology in zebrafish larvae at 72 hpf. (C) Cross-sectional area of cardiac edema in mm^2. (D) Stroke volume, (E) cardiac output and (F) arterial pulse in zebrafish larvae treated with DOX and t-AUCB at 72 hpf. (G and I) Blood velocity and (H and J) diameter for the (G and H) DA and (I and J) PCV of zebrafish. One-way ANOVA followed by Tukey's multiple comparison test was performed to determine the significant differences between groups ($^{+}P<0.05$ vs. control, $^{*}P<0.05$ vs. DOX). DOX, doxorubicin; t-AUCB, 4-[[trans-4-[[(tricyclo[3.3.1.13,7]dec-1-ylamino)carbonyl] amino]cyclohexyl]oxy]-benzoic acid; hpf, hours post-fertilization; DA, dorsal aorta; PCV, posterior cardinal vein.

MSPPOH, at 24 hpf (Fig. 11A). The cardiac and vascular function of zebrafish larvae were then assessed at 72 hpf. Notably, the EET formation inhibitor MSPPOH significantly abolished the protective effect of PTUPB on cardiac edema (Fig. 11B and C), stroke volume (Fig. 11D), and cardiac output (Fig. 11E), as well as the blood velocity of the DA compared with zebrafish treated with DOX and PTUPB (Fig. 11G). While the MSPPOH group did not show a significant change in the diameter of DA, the blood velocity, and the diameter of PCV compared with zebrafish treated with DOX and PTUPB (Fig. 11H-J), the MSPPOH group still did not demonstrate a significant difference from zebrafish treated with DOX alone (Fig. 11H, I, J), suggesting that PTUPB was unable to protect against DOX-induced cardiovascular toxicity in the presence of MSPPOH. However, no significant changes in arterial pulse were observed in zebrafish treated with DOX, PTUPB, or MSPPOH (Fig. 11F). Together, the data in the present study indicated that PTUPB exhibited a cardioprotective effect in

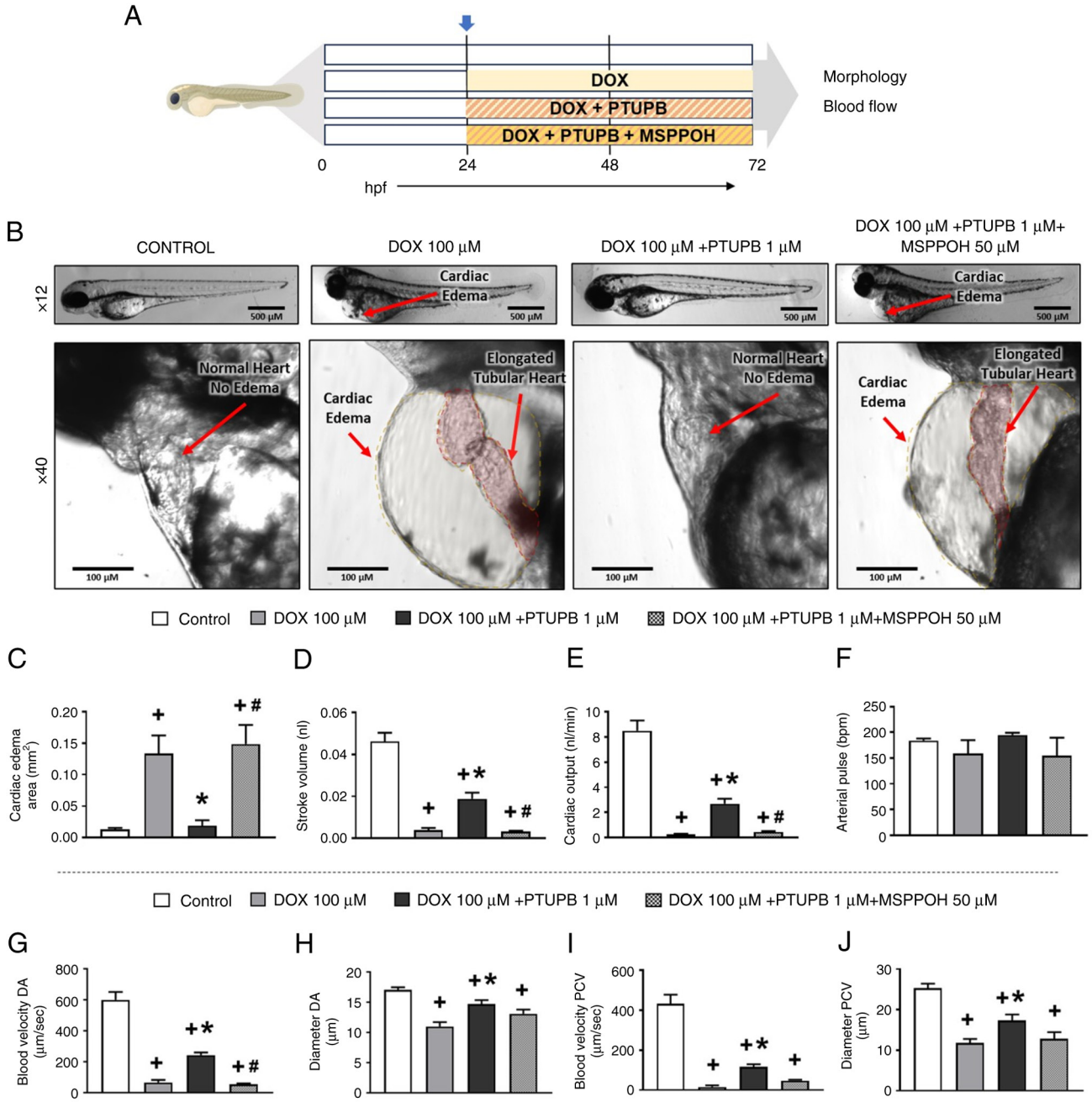

Figure 11. Inhibition of epoxyeicosatrienoic acid formation using MSPPOH abolishes the protective effect of PTUPB against DOX-induced cardiac and vascular dysfunction in zebrafish. (A) Schematic representation of the treatment protocol. (B) Representative images of cardiac morphology in zebrafish larvae at 72 hpf. (C) Cross-sectional area of cardiac edema in mm^2. (D) Stroke volume, (E) cardiac output and (F) arterial pulse in zebrafish larvae treated with DOX and PTUPB with or without MSPPOH at 72 hpf. (G and I) Blood velocity and (H and J) diameter for the (G and H) DA and (I and J) PCV of zebrafish. One-way ANOVA followed by Tukey's multiple comparison test was performed to determine the significant differences between groups ($^{+}P<0.05$ vs. control, $^{*}P<0.05$ vs. DOX, $^{\#}P<0.05$ vs. DOX + PTUPB). MSPPOH, N-methylsulfonyl-6-(2-propargyloxyphenyl)-hexanamide; PTUPB, 4-[5-phenyl-3-[3-[[[[4-(trifluoro methyl)phenyl]amino]carbonyl]amino]propyl]-1H-pyrazol-1-yl]-benzenesulfonamide; hpf, hours post-fertilization; DOX, doxorubicin; DA, dorsal aorta; PCV, posterior cardinal vein.

the zebrafish model of DOX-induced cardiovascular toxicity, mainly through the inhibition of sEH (Fig. 12).

Discussion

A number of previous studies have demonstrated that DOX can detrimentally affect endothelial and vascular function in patients with cancer (5,6). This adverse effect on the endothelial and vascular system might be an antecedent for DOX-induced cardiovascular toxicity (5,6). It may also explain the high incidence rate of cardiovascular disease in DOX-treated patients later in life (5,6). For instance, DOX-treated juvenile and young adult survivors of cancer exhibit decreased endothelial and vascular function, and an increased incidence of future cardiovascular diseases (5,6). While dexrazoxane, a mitigator of DOX-induced cardiotoxicity, effectively reduces DOX-induced cardiotoxicity, a recent report showed that dexrazoxane was ineffective at preventing acute DOX-induced

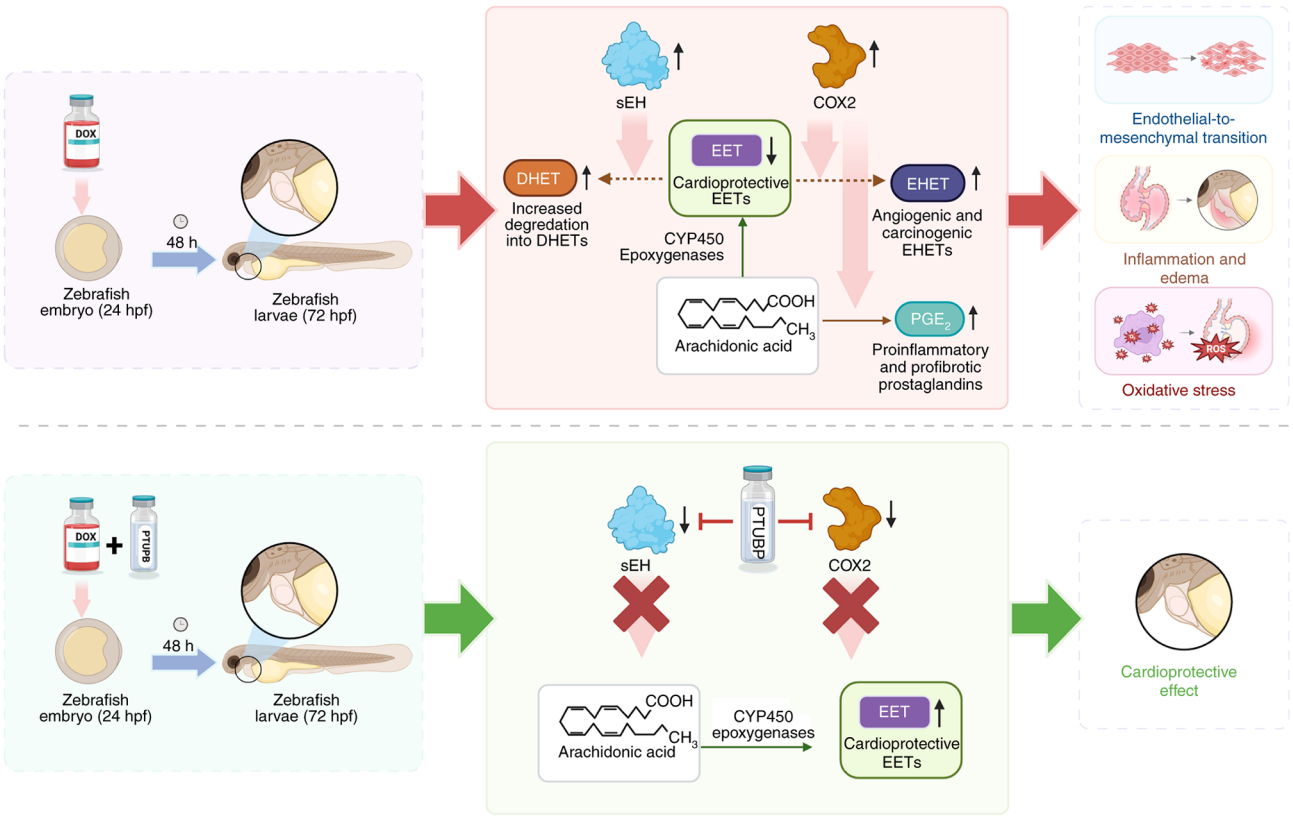

Figure 12. Schematic of the beneficial effect of PTUPB on DOX-induced endothelial, vascular and cardiac toxicity. DOX, doxorubicin; PTUPB, 4-[5-phenyl-3-[3-[[[[4-(trifluoromethyl)phenyl]amino]carbonyl]amino]propyl]-1H-pyrazol-1-yl]-benzenesulfonamide; hpf, hours post-fertilization; DHET, dihydroxyeicosatrienoic acid; sEH, soluble epoxide hydrolase; EET, epoxyeicosatrienoic acid; CYP450, cytochrome P450; COX-2, cyclooxygenase-2; EHET, poxyhydroxyeicosatrienoic acid; PGE_2, prostaglandin E_2; ROS, reactive oxygen species.

endothelial and vascular dysfunction (55). Thus, it is important to identify a novel agent that will help to mitigate DOX-induced endothelial and vascular toxicity.

Since our previous study showed that DOX-induced endothelial and vascular toxicity by suppressing CYP epoxygenase and reducing EETs (20), the present study aimed to test whether increasing EET levels by inhibiting the EET metabolizing enzyme sEH would protect against DOX-induced endothelial and vascular toxicity. However, while suppression of sEH causes EETs to accumulate, and attenuates endothelial, vascular, and cardiac inflammation (23), the chronic suppression of sEH or elevation of EETs increases the metabolism of arachidonic acid to prostaglandins by upregulating the expression of COX-2 (56,57). This effect on COX-2 not only increases the risk of forming inflammatory prostaglandins but can also further metabolize EET into carcinogenic products, EHETs (21). Thus, it is important to use a drug such as PTUPB that boosts EET levels while decreasing the formation of inflammatory and carcinogenic prostaglandins and EHETs (21,35). This is important given that the purpose of the present study was to reduce the adverse effect of DOX without compromising its anticancer activity. Notably, PTUPB is a novel dual inhibitor of sEH and COX-2 (48), exhibiting antitumor effects, and reducing chemotherapy and systemic inflammation-induced multiple organ injury (35,58-60).

While selective COX-2 inhibitors such as celecoxib or rofecoxib have a potential risk of cardiovascular adverse events, which is likely due to reducing the formation of prostaglandin I2 without affecting the levels of thromboxane A2, the former being a potent vasodilator and platelet aggregation inhibitor, and the latter a vasoconstrictor and platelet aggregator (61,62), this was not expected to be the case for PTUPB. Previous studies have shown that PTUPB only reduced the formation of proinflammatory prostaglandin E2 and did not alter the ratio of prostaglandin I2 to thromboxane A2, suggesting that PTUPB has a favorable cardiovascular profile compared with the aforementioned selective COX-2 inhibitors (35,63). While the inhibition of COX-2 may have contributed to potentiating the anticancer effect of DOX (21), it was also expected that a slight inhibition of COX-2 might have been beneficial, at least in part, for DOX-induced cardiotoxicity, probably by maintaining the level of EET and preventing it from being metabolized to EHETs, and by reducing the formation of prostaglandin E2 (59,63).

In the present study, PTUPB was shown to inhibit sEH and COX-2 expression and reduced EndMT in human endothelial cells. The present study also demonstrated that PTUPB reduced DOX-induced vascular toxicity in DOX-administered zebrafish. In addition, evidence suggested that the protective effect of PTUPB against DOX-induced vascular toxicity in zebrafish was associated with downregulation of EndMT and vascular toxicity markers. The results of the present study are consistent with previous studies showing that the dual inhibition of sEH and COX-2 and the elevation of EETs reduce EndMT, improve vascular and endothelial function, and lessen injury in the blood vessels, liver and kidneys (64,65). Conversely, the downregulation of CYP epoxygenase and a reduction in EETs exacerbate

endothelial toxicity, aggravate EndMT, and worsen vascular and cardiac dysfunction (20,66). Thus, the present data suggested that inhibiting EET metabolizing enzymes, such as sEH and COX-2, using PTUPB reduced EndMT and protected against DOX-induced endothelial and vascular toxicity.

Another notable finding in the present study was that PTUPB significantly abolished cardiac edema and improved cardiac function and morphology in zebrafish treated with DOX. This observation was consistent with previous reports demonstrating that sEH inhibitors reduce cardiac inflammation and improve myocardial function and morphology in different preclinical models of cardiac diseases (67,68). It is unclear if this effect of PTUPB on cardiac function and morphology was due to its direct cardioprotective effect or resulted from its beneficial impact on endothelial and vascular function. Nevertheless, the findings of the present study indicate a beneficial effect of PTUPB on DOX-induced cardiovascular toxicity in zebrafish.

The present study also shed light on the contribution of inflammation and oxidative stress to DOX-induced endothelial, vascular, and cardiac toxicity. Notably, inflammation and oxidative stress are vital contributors to EndMT, and endothelial, vascular, and cardiac toxicity (69-73). Equally important was that the inhibition of EET metabolizing enzymes, sEH and COX-2, using PTUPB downregulated inflammation and oxidative stress markers, contributing to the protective effect observed in DOX-induced endothelial, vascular, and cardiac toxicity. The present findings were consistent with previous studies showing that PTUPB reduced mesenchymal cell transition in the lungs, and ameliorated injury in the liver, lungs, and kidneys by abrogating inflammation and oxidative stress (23,44,46,47). Additionally, inhibition of the EET-forming enzyme, CYP epoxygenase, exacerbates DOX-induced EndMT and aggravates inflammation and oxidative stress (20). Thus, it was likely that the inhibition of EET metabolizing enzymes, such as sEH and COX-2, using PTUPB reduced DOX-induced endothelial and vascular toxicity in the zebrafish model by lessening inflammation and oxidative stress.

Given that previous studies have demonstrated that the inhibition of sEH is beneficial to the cardiovascular system (67,68) and that PTUPB is a more selective inhibitor of sEH compared with COX-2 (48), the protective effect of PTUPB on DOX-induced cardiovascular toxicity was likely attributed to the inhibition of sEH. Consistent with this hypothesis, the results of the present study showed that t-AUCB, a selective sEH inhibitor, protected against DOX-induced cardiovascular toxicity. On the other hand, blocking EET synthesis using MSPPOH abolished the beneficial effect of PTUPB on DOX-induced cardiovascular toxicity. In agreement with the present findings, it has been demonstrated that PTUPB improved endothelial dysfunction and reduced blood pressure and renal injury in obese ZSF1 rats, as well as in sorafenib-induced hypertension, likely due to the inhibition of sEH (59,63). These findings, along with the data of the present study, suggested that the preferential inhibition of sEH was likely to be a key contributor to the protective effects of PTUPB on DOX-induced cardiovascular toxicity.

A limitation of the present study was that higher concentrations of PTUPB (2.5 and 5.0 μM) exacerbated DOX-induced endothelial toxicity, suggesting that PTUPB exhibited a concentration-dependent effect, which warrants further investigation. The activity of COX-2 and the formation of prostaglandin E2 were not directly measured in the present study. Although the findings of the present study suggested that PTUPB reduced DOX-induced cardiovascular toxicity, likely due to a reduction in systemic mesenchymal, inflammatory and oxidative stress markers, the present study did not confirm these observations using immune blot analysis. Further investigation is needed to confirm these findings.

In summary, the data of the present study indicated that the inhibition of sEH and COX-2 using PTUPB reduced DOX-induced EndMT and vascular toxicity. PTUPB was also shown to improve cardiac function and morphology in a zebrafish model of DOX-induced cardiovascular toxicity. The data of the present study demonstrated that the protective effect of PTUPB against DOX-induced endothelial and cardiovascular toxicity was associated with downregulation of inflammation and oxidative stress markers. Given that the present study showed that PTUPB enhanced the anticancer effect of DOX, and PTUPB exhibited an antitumor effect and reduced chemotherapy-induced systemic inflammation and multiple organ injury in previous studies (35,58-60), treatment approaches that target sEH and COX-2, such as PTUPB, may help mitigate the detrimental effect of DOX on the cardiovascular system while improving its antitumor activity.

Acknowledgements

The authors would like to thank Ms. Enas Al-Absi and Mr. Ahmad Elwan (Biomedical Research Center, QU Health, Qatar University, Doha, Qatar) for their support with fish care, technical assistance and training.

Funding

The present study was supported by Qatar University Internal (grant no. QUCG-CPH-25/26-754 - Open Access funding provided by Qatar University).

Availability of data and materials

The proteomics data generated in the present study may be found in the ProteomeXchange database under accession number PXD065109 or at the following URL: https://proteomecentral.proteomexchange.org/cgi/GetDataset?ID=PXD065109. The other data generated in the present study may be requested from the corresponding author.

Authors' contributions

ZHM designed the study. ZHM, HD, NAAS LT, MHH and SMY conducted the experiments. ZHM, HD, NAAS, SMY, LT and HCY analysed the data. ZHM, NAAS, HD and HCY wrote the manuscript. All authors have read and approved the final version of the manuscript. ZHM and HD confirm the authenticity of all the raw data.

Ethics approval and consent to participate

Zebrafish studies were conducted in accordance with international guidelines and the policies required by Qatar University

and the Department of Research in the Ministry of Public Health for the use of zebrafish in experimental studies under the approval of the Institutional Animal Care and Use Committee (approval no. QU-IACUC 006/2023-AMM1) and Institutional Biohazard Committee (approval no. QU-IBC-2023/025; both Doha, Qatar).

Patient consent for publication

Not applicable.

Competing interests

The authors declare that they have no competing interests.

References

1. Mohamed AA, Elmancy LY, Abulola SM, Al-Qattan SA, Mohamed Ibrahim MI and Maayah ZH: Assessment of native myocardial T1 mapping for early detection of Anthracycline-induced cardiotoxicity in patients with cancer: A systematic review and meta-analysis. Cardiovasc Toxicol 24: 563-575, 2024.
2. van der Zanden SY, Qiao X and Neefjes J: New insights into the activities and toxicities of the old anticancer drug doxorubicin. FEBS J 288: 6095-6111, 2021.
3. Kirkham AA, Beaudry RI, Paterson DI, Mackey JR and Haykowsky MJ: Curing breast cancer and killing the heart: A novel model to explain elevated cardiovascular disease and mortality risk among women with early stage breast cancer. Prog Cardiovasc Dis 62: 116-126, 2019.
4. Parambil JV, Najim M, Mahmoud M, Abubeker IY, Kartha A, Calaud F, Al-Mohamed A, Al-Mohannadi D, Chandra P and A Yassin M: Breast cancer screening practices in a tertiary care center in the state of qatar: A Cross-sectional survey. Breast Cancer (Dove Med Press) 13: 21-30, 2021.
5. Clayton ZS, Hutton DA, Mahoney SA and Seals DR: Anthracycline Chemotherapy-mediated vascular dysfunction as a model of accelerated vascular aging. Aging Cancer 2: 45-69, 2021.
6. Clayton ZS, Ade CJ, Dieli-Conwright CM and Mathelier HM: A bench to bedside perspective on anthracycline chemotherapy-mediated cardiovascular dysfunction: Challenges and opportunities. A symposium review. J Appl Physiol (1985) 133: 1415-1429, 2022.
7. De Angelis A, Urbanek K, Cappetta D, Piegari E, Ciuffreda LP, Rivellino A, Russo R, Esposito G, Rossi F and Berrino L: Doxorubicin cardiotoxicity and target cells: A broader perspective. Cardiooncology 2: 2, 2016.
8. Kattan LA, Abulola SM, Mohamed Ibrahim MI and Maayah ZH: Anthracyclines-induced vascular endothelial dysfunction in cancer patients and survivors using brachial Flow-mediated dilation (FMD) tool: A systematic review and Meta-analysis. Cardiovasc Toxicol 25: 692-718, 2025.
9. Imig JD: Epoxygenase metabolites. Epithelial and vascular actions. Mol Biotechnol 16: 233-251, 2000.
10. Zeldin DC: Epoxygenase pathways of arachidonic acid metabolism. J Biol Chem 276: 36059-36062, 2001.
11. Node K, Ruan XL, Dai J, Yang SX, Graham L, Zeldin DC and Liao JK: Activation of Galpha s mediates induction of tissue-type plasminogen activator gene transcription by epoxyeicosatrienoic acids. J Biol Chem 276: 15983-15989, 2001.
12. Chen JK, Capdevila J and Harris RC: Cytochrome p450 epoxygenase metabolism of arachidonic acid inhibits apoptosis. Mol Cell Biol 21: 6322-6331, 2001.
13. Pomposiello SI, Carroll MA, Falck JR and McGiff JC: Epoxyeicosatrienoic acid-mediated renal vasodilation to arachidonic acid is enhanced in SHR. Hypertension 37: 887-893, 2001.
14. Pratt PF, Li P, Hillard CJ, Kurian J and Campbell WB: Endothelium-independent, ouabain-sensitive relaxation of bovine coronary arteries by EETs. Am J Physiol Heart Circ Physiol 280: H1113-H1121, 2001.
15. Zhang Y, Oltman CL, Lu T, Lee HC, Dellsperger KC and VanRollins M: EET homologs potently dilate coronary microvessels and activate BK(Ca) channels. Am J Physiol Heart Circ Physiol 280: H2430-H2440, 2001.
16. Campbell WB: New role for epoxyeicosatrienoic acids as Anti-inflammatory mediators. Trends Pharmacol Sci 21: 125-127, 2000.
17. Node K, Huo Y, Ruan X, Yang B, Spiecker M, Ley K, Zeldin DC and Liao JK: Anti-inflammatory properties of cytochrome P450 Epoxygenase-derived eicosanoids. Science 285: 1276-1279, 1999.
18. Levick SP, Loch DC, Taylor SM and Janicki JS: Arachidonic acid metabolism as a potential mediator of cardiac fibrosis associated with inflammation. J Immunol 178: 641-646, 2007.
19. Althurwi HN, Maayah ZH, Elshenawy OH and El-Kadi AO: Early changes in cytochrome P450s and their associated arachidonic acid metabolites play a crucial role in the initiation of cardiac hypertrophy induced by isoproterenol. Drug Metab Dispos 43: 1254-1266, 2015.
20. Dhulkifle H, Therachiyil L, Hasan MH, Sayed TS, Younis SM, Korashy HM, Yalcin HC and Maayah ZH: Inhibition of cytochrome P450 epoxygenase promotes Endothelium-to-mesenchymal transition and exacerbates doxorubicin-induced cardiovascular toxicity. Mol Biol Rep 51: 859, 2024.
21. Rand AA, Rajamani A, Kodani SD, Harris TR, Schlatt L, Barnych B, Passerini AG and Hammock BD: Epoxyeicosatrienoic acid (EET)-stimulated angiogenesis is mediated by epoxy hydroxyeicosatrienoic acids (EHETs) formed from COX-2. J Lipid Res 60: 1996-2005, 2019.
22. Maayah ZH, Elshenawy OH, Althurwi HN, Abdelhamid G and El-Kadi AO: Human fetal ventricular cardiomyocyte, RL-14 cell line, is a promising model to study drug metabolizing enzymes and their associated arachidonic acid metabolites. J Pharmacol Toxicol Methods 71: 33-41, 2015.
23. Duan JX, Guan XX, Cheng W, Deng DD, Chen P, Liu C, Zhou Y, Hammock BD and Yang HH: COX-2/sEH-Mediated macrophage activation is a target for pulmonary protection in mouse models of chronic obstructive pulmonary disease. Lab Invest 104: 100319, 2024.
24. Maayah ZH, El Gendy MAM, El-Kadi AO and Korashy HM: Sunitinib, a tyrosine kinase inhibitor, induces cytochrome P450 1A1 gene in human breast cancer MCF7 cells through ligand-independent aryl hydrocarbon receptor activation. Arch Toxicol 87: 847-856, 2013.
25. Pan JA, Zhang H, Lin H, Gao L, Zhang HL, Zhang JF, Wang CQ and Gu J: Irisin ameliorates doxorubicin-induced cardiac perivascular fibrosis through inhibiting endothelial-to-mesenchymal transition by regulating ROS accumulation and autophagy disorder in endothelial cells. Redox Biol 46: 102120, 2021.
26. Liu Y, Asnani A, Zou L, Bentley VL, Yu M, Wang Y, Dellaire G, Sarkar KS, Dai M, Chen HH, *et al*: Visnagin protects against doxorubicin-induced cardiomyopathy through modulation of mitochondrial malate dehydrogenase. Sci Transl Med 6: 266ra170, 2014.
27. Zakaria Z, Suleiman M and Benslimane F: Imatinib- and ponatinib-mediated cardiotoxicity in zebrafish embryos and H9c2 cardiomyoblasts. Mol Med Rep 30: 187, 2024.
28. Westerfield M: The zebrafish book: A guide for the laboratory use of zebrafish (Danio rerio). 4th edition. University of Oregon Press, Eugene, 2000.
29. Yalcin HC, Amindari A, Butcher JT, Althani A and Yacoub M: Heart function and hemodynamic analysis for zebrafish embryos. Dev Dyn 246: 868-880, 2017.
30. Strykowski JL and Schech JM: Effectiveness of recommended euthanasia methods in larval zebrafish (Danio rerio). J Am Assoc Lab Anim Sci 54: 81-84, 2015.
31. Leary S, Underwood W, Anthony R and Cartner S: AVMA Guidelines for the Euthanasia of Animals: 2020 Edition. Veterinary A and Association M (eds.), 2020.
32. Lam PY, Kutchukian P, Anand R, Imbriglio J, Andrews C, Padilla H, Vohra A, Lane S, Parker DL Jr, Cornella Taracido I, *et al*: Cyp1 inhibition prevents Doxorubicin-induced cardiomyopathy in a zebrafish Heart-Failure model. Chembiochem 21: 1905-1910, 2020.
33. Asnani A, Zheng B, Liu Y, Wang Y, Chen HH, Vohra A, Chi A, Cornella-Taracido I, Wang H, Johns DG, *et al*: Highly potent visnagin derivatives inhibit Cyp1 and prevent doxorubicin cardiotoxicity. JCI Insight 3: e96753, 2018.
34. Huang B, Cui YQ, Guo WB, Yang L and Miao AJ: Waterborne and dietary accumulation of well-dispersible hematite nanoparticles by zebrafish at different life stages. Environ Pollut 259: 113852, 2020.
35. Zhang G, Panigrahy D, Hwang SH, Yang J, Mahakian LM, Wettersten HI, Liu JY, Wang Y, Ingham ES, Tam S, *et al*: Dual inhibition of cyclooxygenase-2 and soluble epoxide hydrolase synergistically suppresses primary tumor growth and metastasis. Proc Natl Acad Sci USA 111: 11127-11132, 2014.
36. Dhulkifle H, Sayed TS, Abunada HH, Abulola SM, Alhoshani A, Korashy HM and Maayah ZH: 6-Formylindolo(3,2-b)carbazole dampens inflammation and reduces Endotoxin-induced kidney injury via Nrf2 activation. Chem Res Toxicol 36: 552-560, 2023.

37. Livak KJ and Schmittgen TD: Analysis of relative gene expression data using real-time quantitative PCR and the 2(-Delta Delta C(T)) method. Methods 25: 402-408, 2001.
38. Therachiyil L, Peerapen P, Younis SM, Ahmad A, Thongboonkerd V, Uddin S and Korashy HM: Proteomic insight towards key modulating proteins regulated by the aryl hydrocarbon receptor involved in ovarian carcinogenesis and chemoresistance. J Proteomics 295: 105108, 2024.
39. Korashy HM, Maayah ZH, Al Anazi FE, Alsaad AM, Alanazi IO, Belali OM, Al-Atawi FO and Alshamsan A: Sunitinib inhibits breast cancer cell proliferation by inducing apoptosis, Cell-cycle arrest and DNA repair while inhibiting NF-κB signaling pathways. Anticancer Res 37: 4899-4909, 2017.
40. Cox J, Neuhauser N, Michalski A, Scheltema RA, Olsen JV and Mann M: Andromeda: A peptide search engine integrated into the MaxQuant environment. J Proteome Res 10: 1794-1805, 2011.
41. Tyanova S, Temu T and Cox J: The MaxQuant computational platform for mass Spectrometry-based shotgun proteomics. Nature Protocols 11: 2301-2319, 2016.
42. Cox J, Hein MY, Luber CA, Paron I, Nagaraj N and Mann M: Accurate Proteome-wide label-free quantification by delayed normalization and maximal peptide ratio extraction, termed MaxLFQ. Mol Cell Proteomics 13: 2513-2526, 2014.
43. Hourani W, Deb PK, Alhawamdeh M, Al-Shari N, Borah P, Dahabiyeh LA, Jaber AY, P N, S S, Dasappa JP and Venugopala KN: Anticancer and cyclooxygenase inhibitory activity of benzylidene derivatives of fenobam and its thio analogues. Curr Med Chem: 2024: December 16, 2024 (Epub ahead of print).
44. Zhang CY, Guan XX, Song ZH, Jiang HL, Liu YB, Chen P, Duan JX and Zhou Y: COX-2/sEH dual inhibitor PTUPB attenuates Epithelial-mesenchymal transformation of alveolar epithelial cells via Nrf2-mediated inhibition of TGF-β1/smad signaling. Oxid Med Cell Longev 2022: 5759626, 2022.
45. Roche C, Besnier M, Cassel R, Harouki N, Coquerel D, Guerrot D, Nicol L, Loizon E, Remy-Jouet I, Morisseau C, *et al*: Soluble epoxide hydrolase inhibition improves coronary endothelial function and prevents the development of cardiac alterations in obese Insulin-resistant mice. Am J Physiol Heart Circ Physiol 308: H1020-H1029, 2015.
46. Zhang YF, Sun CC, Duan JX, Yang HH, Zhang CY, Xiong JB, Zhong WJ, Zu C, Guan XX, Jiang HL, *et al*: A COX-2/sEH dual inhibitor PTUPB ameliorates cecal ligation and Puncture-induced sepsis in mice via Anti-inflammation and Anti-oxidative stress. Biomed Pharmacother 126: 109907, 2020.
47. Fishbein A, Wang W, Yang H, Yang J, Hallisey VM, Deng J, Verheul SML, Hwang SH, Gartung A, Wang Y, *et al*: Resolution of eicosanoid/cytokine storm prevents carcinogen and inflammation-initiated hepatocellular cancer progression. Proc Natl Acad Sci USA 117: 21576-21587, 2020.
48. Hwang SH, Wagner KM, Morisseau C, Liu JY, Dong H, Wecksler AT and Hammock BD: Synthesis and structure-activity relationship studies of urea-containing pyrazoles as dual inhibitors of cyclooxygenase-2 and soluble epoxide hydrolase. J Med Chem 54: 3037-3050, 2011.
49. Lesk AM and Chothia C: How different amino acid sequences determine similar protein structures: The structure and evolutionary dynamics of the globins. J Mol Biol 136: 225-230, 231-270, 1980.
50. Todd AE, Orengo CA and Thornton JM: Evolution of function in protein superfamilies, from a structural perspective. J Mol Biol 307: 1113-1143, 2001.
51. Xie L and Bourne PE: Functional coverage of the human genome by existing structures, structural genomics targets, and homology models. PLoS Comput Biol 1: e31, 2005.
52. Cronin A, Mowbray S, Durk H, Homburg S, Fleming I, Fisslthaler B, Oesch F and Arand M: The N-terminal domain of mammalian soluble epoxide hydrolase is a phosphatase. Proc Natl Acad Sci USA 100: 1552-1557, 2003.
53. Al-Shar'I NA, Al-Balas QA, Al-Waqfi RA, Hassan MA, Alkhalifa AE and Ayoub NM: Discovery of a nanomolar inhibitor of the human glyoxalase-I enzyme using structure-based poly-pharmacophore modelling and molecular docking. J Comput Aided Mol Des 33: 799-815, 2019.
54. Rouzer CA and Marnett LJ: Structural and chemical biology of the interaction of cyclooxygenase with substrates and non-steroidal Anti-inflammatory drugs. Chem Rev 120: 7740-7781, 2020.
55. Bosman M, Kruger DN, Favere K, De Meyer GRY, Franssen C, Van Craenenbroeck EM and Guns PJ: Dexrazoxane does not mitigate early vascular toxicity induced by doxorubicin in mice. PLoS One 18: e0294848, 2023.
56. Kim HS, Kim SK and Kang KW: Differential effects of sEH inhibitors on the proliferation and migration of vascular smooth muscle cells. Int J Mol Sci 18: 2683, 2017.
57. Park SK, Herrnreiter A, Pfister SL, Gauthier KM, Falck BA, Falck JR and Campbell WB: GPR40 is a low-affinity epoxyeicosatrienoic acid receptor in vascular cells. J Biol Chem 293: 10675-10691, 2018.
58. Yang HH, Duan JX, Liu SK, Xiong JB, Guan XX, Zhong WJ, Sun CC, Zhang CY, Luo XQ, Zhang YF, *et al*: A COX-2/sEH dual inhibitor PTUPB alleviates lipopolysaccharide-induced acute lung injury in mice by inhibiting NLRP3 inflammasome activation. Theranostics 10: 4749-4761, 2020.
59. Jankiewicz WK, Barnett SD, Stavniichuk A, Hwang SH, Hammock BD, Belayet JB, Khan AH and Imig JD: Dual sEH/COX-2 inhibition using PTUPB-A promising approach to Antiangiogenesis-induced nephrotoxicity. Front Pharmacol 12: 744776, 2021.
60. Zhang CY, Duan JX, Yang HH, Sun CC, Zhong WJ, Tao JH, Guan XX, Jiang HL, Hammock BD, Hwang SH, *et al*: COX-2/sEH dual inhibitor PTUPB alleviates bleomycin-induced pulmonary fibrosis in mice via inhibiting senescence. FEBS J 287: 1666-1680, 2020.
61. Cheng Y, Austin SC, Rocca B, Koller BH, Coffman TM, Grosser T, Lawson JA and FitzGerald GA: Role of prostacyclin in the cardiovascular response to thromboxane A2. Science 296: 539-541, 2002.
62. Schmelzer KR, Inceoglu B, Kubala L, Kim IH, Jinks SL, Eiserich JP and Hammock BD: Enhancement of antinociception by coadministration of nonsteroidal anti-inflammatory drugs and soluble epoxide hydrolase inhibitors. Proc Natl Acad Sci USA 103: 13646-13651, 2006.
63. Khan MAH, Hwang SH, Barnett SD, Stavniichuk A, Jankiewicz WK, Hammock BD and Imig JD: Multitarget molecule, PTUPB, to treat diabetic nephropathy in rats. Br J Pharmacol 178: 4468-4484, 2021.
64. Wu H, Li D, Zhang CY, Huang LL, Zeng YJ, Chen TG, Yu K, Meng JW, Lin YX, Guo R, *et al*: Restoration of ARA metabolic disorders in vascular smooth muscle cells alleviates intimal hyperplasia. Eur J Pharmacol 983: 176824, 2024.
65. Zhang CY, Tan XH, Yang HH, Jin L, Hong JR, Zhou Y and Huang XT: COX-2/sEH dual inhibitor alleviates hepatocyte senescence in NAFLD mice by restoring autophagy through Sirt1/PI3K/AKT/mTOR. Int J Mol Sci 23: 8267, 2022.
66. Zhang Y, Lu J, Huang S, Zhang Y, Liu J, Xu Y, Yao B and Wang X: CYP2J deficiency leads to cardiac injury and presents dual regulatory effects on cardiac function in rats. Toxicol Appl Pharmacol 473: 116610, 2023.
67. Dai N, Yang C, Fan Q, Wang M, Liu X, Zhao H and Zhao C: The Anti-inflammatory effect of soluble epoxide hydrolase inhibitor and 14, 15-EET in kawasaki disease through PPARgamma/STAT1 signaling pathway. Front Pediatr 8: 451, 2020.
68. Maayah ZH, Abdelhamid G, Elshenawy OH, El-Sherbeni AA, Althurwi HN, McGinn E, Dawood D, Alammari AH and El-Kadi AOS: The role of soluble epoxide hydrolase enzyme on Daunorubicin-mediated cardiotoxicity. Cardiovasc Toxicol 18: 268-283, 2018.
69. Cho JG, Lee A, Chang W, Lee MS and Kim J: Endothelial to mesenchymal transition represents a key link in the interaction between inflammation and endothelial dysfunction. Front Immunol 9: 294, 2018.
70. Montorfano I, Becerra A, Cerro R, Echeverría C, Sáez E, Morales MG, Fernández R, Cabello-Verrugio C and Simon F: Oxidative stress mediates the conversion of endothelial cells into myofibroblasts via a TGF-β1 and TGF-β2-dependent pathway. Lab Invest 94: 1068-1082, 2014.
71. Li J, Xiong J, Yang B, Zhou Q, Wu Y, Luo H, Zhou H, Liu N, Li Y, Song Z and Zheng Q: Endothelial cell apoptosis induces TGF-β Signaling-dependent host Endothelial-mesenchymal transition to promote transplant arteriosclerosis. Am J Transplant 15: 3095-3111, 2015.
72. Zhou K, Tian KJ, Yan BJ, Gui DD, Luo W, Ren Z, Wei DH, Liu LS and Jiang ZS: A promising field: regulating imbalance of EndMT in cardiovascular diseases. Cell Cycle 20: 1477-1486, 2021.
73. Perez L, Munoz-Durango N, Riedel CA, Echeverría C, Kalergis AM, Cabello-Verrugio C and Simon F: Endothelial-to-mesenchymal transition: Cytokine-mediated pathways that determine endothelial fibrosis under inflammatory conditions. Cytokine Growth Factor Rev 33: 41-54, 2017.